# DEVELOPMENT OF A CYBER-PHYSICAL TESTBED FOR RESILIENT EXTRA-TERRESTRIAL HABITATS

by

**Jaewon Park**

**A Thesis**

*Submitted to the Faculty of Purdue University*

*In Partial Fulfillment of the Requirements for the degree of*

**Master of Science in Mechanical Engineering**

School of Mechanical Engineering

West Lafayette, Indiana

May 2022

**THE PURDUE UNIVERSITY GRADUATE SCHOOL**
**STATEMENT OF COMMITTEE APPROVAL**

**Dr. Davide Ziviani, Chair**
School of Mechanical Engineering

**Dr. Ilias Bilionis**
School of Mechanical Engineering

**Dr. Shirley Dyke**
School of Mechanical Engineering

**Approved by:**
Dr. Nicole L. Key

*Dedicated to everyone who supported me through this*

# ACKNOWLEDGMENTS

This work is funded by NASA under grant or cooperative agreement award number 80NSSC19K1076.

# TABLE OF CONTENTS

# LIST OF TABLES

# LIST OF FIGURES

# NOMENCLATURE

**Symbols:**

| | |
|---|---|
| $A$ | Area [m$^2$] |
| $K$ | Discharge coefficient [-] |
| $L$ | Length [m] |
| $\dot{m}$ | Mass flow rate [kg/s] |
| $\mu$ | Viscosity [Pa-s] |
| $\overline{Nu}$ | Nusselt number [-] |
| $p$ | Pressure [Pa] |
| $Pr$ | Prandtl number [-] |
| $Q$ | Volumetric flow rate [m$^3$/s] |
| $Ra$ | Rayleigh's number [-] |
| $Re$ | Reynolds number [-] |
| $\rho$ | Density [kg/m$^3$] |
| $T$ | Temperature [°C] |

**Abbreviations:**

| | |
|---|---|
| CPT | Cyber-physical testbed |
| ECLSS | Environmental control life support system |
| IE | Interior environment |
| ISS | International space station |
| MCVT | Modular coupled virtual testbed |
| PSI | Predictive stability and performance indicators |
| RETHi | Resilient Extra-Terrestrial Habitat institute |
| SoS | System of systems |
| SPL | Structural protective layer |
| SS | Structural system |

**Subscripts:**

| | |
|---|---|
| $L$ | Length |
| $N$ | Standard condition property |
| $t$ | Tube |

# ABSTRACT

Establishing permanent and sustainable human settlements outside Earth presents numerous challenges. The Resilient Extra-Terrestrial Habitat Institute (RETHi) has been established to advance the fundamental knowledge needed to enable and design resilient habitats in deep space, that will adapt, absorb, and rapidly recover from expected and unexpected disruptions without fundamental changes in function or sacrifices in safety.

Future extra-terrestrial habitats will rely on several subsystems working synergistically to ensure adequate power supply, life support to crew members, manage extreme environmental conditions, and monitor the health status of the equipment. To study extra-terrestrial habitats, a combination of modeling approaches and experimental validations is necessary, but deep-space conditions cannot be entirely reproduced in a laboratory setting (*e.g.*, micro-gravity effects). To this end, real-time multi-physics cyber-physical testing is a novel approach of simulating and evaluating complex system-of-systems (SoS) that has been applied to investigate the behavior of extra-terrestrial habitats under different scenarios (*e.g.*, meteorite strikes). One of the most critical components which determines the success of the cyber-physical testbed is the transfer system serving as an interface between the physical and cyber substructures.

Through this work, a dedicated thermal transfer system has been designed and constructed to provide realistic thermal boundary conditions to the physical habitat according to the real-time simulation results from cyber substructure of the habitat. The extreme temperatures to be found at the interface between the external protective layer of the habitat (cyber) and the interior structural elements (physical) are emulated by means of a cryogenic chiller and an array of cooled panels that cover a dome-style structure. Moreover, the overall architecture of the cyber-physical testbed, the partitioning of the virtual and physical environments, and interface schemes were also established. The experimental results obtained from the thermal transfer system prototype setup were analyzed and interpreted to generate meaningful recommendations for future development and application of the full-sized testbed.

# 1. INTRODUCTION

## 1.1 Motivation

Humanity's inexhaustible curiosity and passion for technological advancement has enabled us to explore and inhabit some of the most rugged places on Earth. Our civilization has consistently dealt with the scarcity of resources and environmental threats such as extreme climate conditions. Being the user of intelligence, humanity has managed to reduce the influence of natural determinants on our settlements over time [1] and found innovative ways to sustain ourselves notwithstanding the surroundings. Sparked by the same curiosity and future necessities, deep space human exploration beyond the Moon or Mars will be one of the next challenges to tackle.

During the recent years of space travel and exploration, astronauts have relied on relatively small spaceships and the mission profiles were of short time (*e.g.*, several months). Considering that the average duration of International Space Station (ISS) missions is about four to six months [2], mankind has yet to experience sustained long-term settlements in extra-terrestrial environments. The necessity for long-term space habitats is gaining growing attention for various reasons ranging from preparation for long-term space experiments, service as replenishment points for deeper space explorations, to commercialization of space tourisms [3]. To achieve this next milestone in the age of space exploration, humans are tasked to deal with unfamiliar situations both externally, from physical stressors such as meteorite events or irregular light cycles, and internally, from social and psychological stressors such as loneliness and disconnection from natural world [4]. Specifically for lunar habitat, Casanova and Sureda [5] published a comprehensive report that outlines a wide range of potential benefits and difficulties for constructing habitats on the Moon. As these issues are often interactive and interdisciplinary, a collaborative work among researchers and scholars from various fields of specialty is necessary. To this end, the NASA Space Technology Mission Directorate's (SpaceTech) Lunar Surface Innovation Initiative (LSII) is developing technologies needed for lunar surface exploration within the Lunar Surface Innovation Consortium (LSIC) [6]. In addition, to enable exploration missions beyond the Moon and Mars, NASA selected two new Space Technology Research Institutes (STRIs) to advance space habitats designs using resilient systems. The two instates selected were the Habitats Optimized Missions of Exploration (HOME) [7] and the Resilient Extra-Terrestrial Habitats Institute (RETHi) [8][9].

## 1.2 Resilient Extra-Terrestrial Habitat Institute

The Resilient Extra-Terrestrial Habitat Institute (RETHi) has been established to advance the fundamental knowledge needed to enable and design resilient habitats in deep space, that will adapt, absorb, and rapidly recover from expected and unexpected disruptions without significant changes in functionalities or sacrifices in safety. These disruptions include a wide range of scenarios from periodic variation of solar irradiation due to a planet's rotations to more complex situations involving a meteorite impact on a physical structure and potential emerging faults of the habitat. Under these circumstances, resilient habitats shall rely on subsystems working synergistically to ensure adequate power supply, life support to crew members, manage extreme environmental conditions, and monitor the health status of the equipment.

RETHi has been developing computational models of system-of-systems (SoS) including multiple subsystems such as structural mechanical and thermal system, power generation system, Environmental Control Life Support System (ECLSS) and exterior environment system to conduct research on designing and operating resilient and autonomous extra-terrestrial settlements. This numerical simulation platform provides researchers with the opportunity to simulate nearly infinite number of case scenarios and investigate ways to improve the resilience, anticipating and adapting to possible threats, and awareness, detecting and diagnosing issues, of the future habitats.

The success of such investigation is heavily dependent on the capacity of the numerical models to capture accurate physical behaviors. However, experimentally validating these numerical models represents a great challenge as many deep-space conditions and scenarios cannot be entirely reproduced in a laboratory setting (*e.g.,* micro-gravity effects, meteorite strikes, etc.). Therefore, an innovative method to validate these models without necessarily creating all the extra-terrestrial conditions is needed and warrants further research efforts.

## 1.3 Challenges of Cyber-Physical Testing

Real-time multi-physics cyber-physical testing is a novel approach of simulating and evaluating complex system-of-systems (SoS) where full-scale testing and validation are very expensive and traditionally done with tremendous constraints in lab settings. In the literature, several examples of real-time hybrid simulation methods can be found. For instance, Li et al. [10] developed a geographically distributed real-time hybrid simulations to examine effect of earthquake on two-story shear beam structure. Wang et al. [11] conducted system-level analysis on a four-story building with one beam subject to direct fire. In addition, Whyte et al. [12] proposed adding thermal degrees of freedom and temperature loads to the conventional approach of structural-mechanical hybrid testing. As real-time hybrid simulations are designed to capture rate dependent behavior in physical substructure, it is critical to ensure steady and undisturbed signal communication between virtual and physical subsystems. While researchers choose to partition the most interesting or the least well-known part of the system for physical investigation, the overall fidelity of the numerical model representing the rest of the system has substantial impact on the success of the simulation. Recent technological advances in computational hardware have enabled researchers to run more accurate, higher-order models in real-time. Often, a considerable amount of effort is put into developing the numerical models as in [13], modeling not only the physics of both cyber and physical substructure but also sensor dynamics and holistic interactions with control and security systems. Models with such depth of complexity and accuracy can be also used in a standalone manner as a theoretical reference system for post-evaluation of hybrid testing results. However, when real-time hybrid simulations are conducted for multi-physics systems at high sampling rates, low-order or mid-order numerical models are still widely used with or without a multi-rate simulation approach discussed in [14].

Due to their complex nature, real-time hybrid simulation tests can vary in stability and performance depending on how they are configured, especially by partitioning choices. Therefore, it is advisable to prepare a procedure to quantify how safe and reliable the tests are. In [15], predictive stability and performance indicators (PSI) were suggested as design tools to optimize simulation configurations. [16] presented a framework for developing a method for quantifying, estimating, and predicting uncertainty both during and at the end of real-time hybrid simulations. Conventionally, real-time hybrid simulations have been applied to evaluate dynamics of structural mechanical systems. In this case, a hydraulic actuator or a shake table serves as the transfer system enforcing boundary conditions at the interface between physical and virtual systems. Forces and displacements are enforced interface conditions for a structurally partitioned system. Accurate measurements of these conditions are the key requirement for realistic simulations results [17]. Depending on sensors, for example, thermocouples in systems with fast dynamic behavior can output delayed measurement in capturing the true physical states [18]. Research efforts such as Lin et al. [19] and Maghareh et al. [20] suggested that particular care should be given to properly design transfer systems and their control schemes. For thermally coupled hybrid simulation tests, stability of simulation can be achieved by considering physical parameters from both numerical and physical substructure for solving balance equations as in [21]. Renard et al. [22] explored a novel way to design hybrid fire testing so that actuator system can be properly controlled with the help of an adaptive controller without explicit information of element position. For the hybrid simulations involving thermal systems and interfaces, the RETHi team decided to employ temperature and heat flux as the interfaces conditions to be enforced. A similar approach was taken in [11] to analyze the impact of fire on structural beams, where a simple but accurate parametric model for fire in building developed in [23] was used to obtain fire temperature curve to be imposed as thermal boundary to the physical substructure. Although the researchers used temperature as the input to the physical substructure, the setup was limited to only one-way coupling between the physical and numerical substructure.

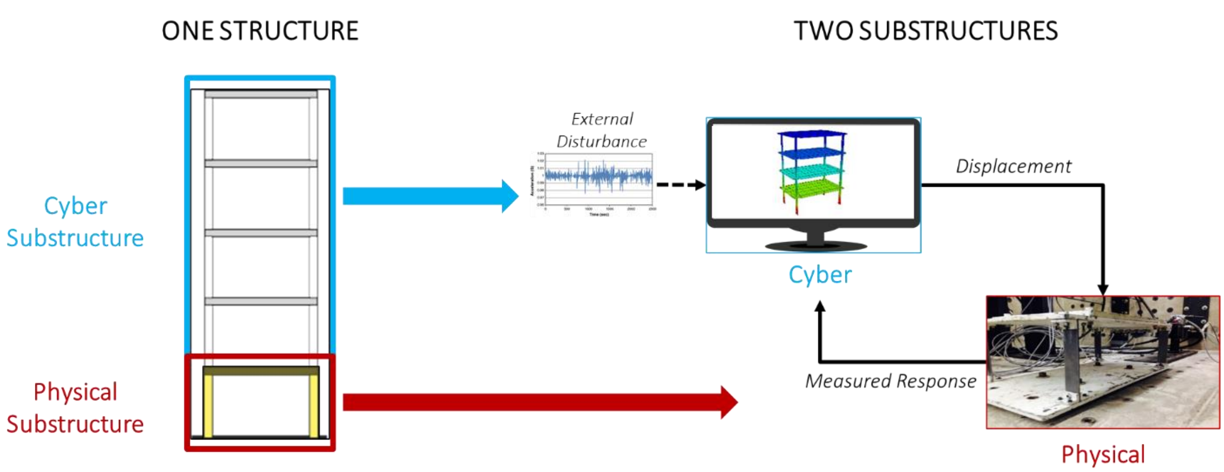


Figure 1. Example of cyber-physical testing architecture for structural mechanical problems (Courtesy of Herta Montoya, RETHi)

## 1.4 Thesis Objectives and Approach

The overarching goal of this study is to develop an appropriate thermal transfer system for the purpose of conducting a real-time hybrid simulation for validating extra-terrestrial habitat models where full-scale tests are impossible. To accomplish the research goals, the following main research tasks have been identified within this work:

- Review the scope of simulation case scenarios involving thermally induced disturbances.
- Understand the high-level CPT architecture, including the current approach of partitioning habitat subsystems into the physical, cyber, and transfer system substructures.
- Develop and optimize the design of thermal transfer system through numerical simulations according to the requirements set by RETHi team.
- Build and test the performance of proposed thermal transfer system in the lab setting to make appropriate adjustment to the design.
- Perform small-scale experiments with the prototype thermal transfer system to collect data, which can be analyzed to generate meaningful feedback to improve the full-size testing under development.

This work is organized in 4 chapters to address the research tasks outlined. Chapter 2 provides an overview of the CPT framework by dividing it into cyber, physical, and transfer system substructure. The definitions and qualitative performance requirements of each substructure are provided. Chapter 3 describes the development of thermal transfer system, one of subsystems of the transfer system substructure. The process of design and optimization of the thermal transfer system is discussed in depth with experimental, performance mapping data. Early efforts of controller development and small-scale testing are described in addition. Finally, Chapter 4 summarizes the key findings of the research and details the challenges encountered and directions for future work.

# 2. INTRODUCTION TO CYBER PHYSICAL TESTING AND MCVT

## 2.1 Modular Coupled Virtual Testbed (MCVT)

The Cyber-Physical Testbed (CPT), real-time simulation environment developed by RETHi, is based on the architecture of the Modular Coupled Virtual Testbed (MCVT), also developed by RETHi. The different MCVT subsystems are partitioned into cyber and physical components for the CPT [24]. The current stage of the CPT includes the following main subsystems: Structural System, Power System, ECLSS, Interior Environment, Structural Protective Layer, and Exterior Environment. The partitioning and clustering of these MCVT subsystems are shown in Table 1 with brief descriptions. Figure 2 summarizes the interaction between the subsystems. Physical subsystems can interact with each other through physical coupling the lab environment, and cyber subsystems can interact through numerical simulation environment. The coupling between the physical and cyber substructure is then completed by the help of transfer systems. As the current CPT has its emphasis on thermal scenarios, the thermal transfer system closes the feedback loop between physical and cyber substructures. Additional transfer systems are to be added to increase the number of freedoms (*e.g.*, mechanical). MCVT aims to include realistic models of these testbed transfer systems and replicate the dynamics and controls needed to enforce boundary conditions between the partitioned cyber and physical components.

Table 1. Cyber-physical partitioning of subsystems and brief descriptions

| Subsystems | Substructure | Description |
|---|---|---|
| **Structural System** | Physical | Supporting beams, structural layer between protective layer and interior environment |
| **Interior Environment** | Physical | Air, equipment, crew quarters |
| **ECLSS** | Physical | Temperature and pressure control |
| **Command and Control** | Physical | Decision making by human and algorithm |
| **Structural Protective Layer** | Cyber | Extraterrestrial materials *e.g.,* lunar regolith |
| **Power System** | Cyber | Power generation and distribution *e.g.,* solar PV |
| **Agent System** | Cyber | Robotic agent for diagnosis and maintenance |
| **Disturbance** | Cyber | Simulation of dust particles, solar radiation, meteorite impacts |
| **Thermal Transfer System** | Transfer | Bridge between structural system and structural protective layer |

*Notes: MCVT is being developed to include all subsystems regardless of substructure portioning for standalone virtual simulation.*

— Physical interaction

— Cyber interaction

Systems receiving signals

Systems sending signals

| Subsystems | Structural System | Interior Environment | ECLSS | Command and Control | Structural Protective Layer | Power System | Agent System | Disturbance |
|---|---|---|---|---|---|---|---|---|
| Structural System | | x | | x | x | x | x | |
| Interior Environment | x | | x | | | x | | |
| ECLSS | | x | | x | | x | x | |
| Command and Control | | | | | | | x | |
| Structural Protective Layer | x | | | x | | x | x | |
| Power System | x | x | x | x | x | | x | |
| Agent System | x | | x | x | x | x | | |
| Disturbance | x | x | x | | x | x | | |

Figure 2. Design structure matrix for the Cyber-Physical Testbed (CPT). Interactions between physical and cyber substructures are conducted through the help of transfer systems.

One of the major goals for the CPT is to replicate meteorite impact scenarios based on their severity as thermal problems. In the MCVT Scenarios currently under development, the meteorite directly impacts the SPL, causing cascading effects for the structural dome and interior environment. In Figure 2, it is shown that the SPL will be part of the cyber environment. In contrast, the structural dome (mechanical and thermal) and interior environment will be physical components in the laboratory. At this time, RETHi does not plan on reproducing mechanical impact forces through these layers of subsystems but does plan to replicate the thermal impact through imposing thermal boundary conditions on the interface between physical and cyber substructures at different magnitudes. For example, in MCVT Scenarios, the SPL experiences major damage due to meteorite impact as illustrated in Figure 3. The removal of the protective material, including lunar regolith and any other material, will result in temperature changes for the surface of the structural dome in the damaged area. The thermal transfer system will be responsible for enforcing the temperature changes physically in the lab environment.

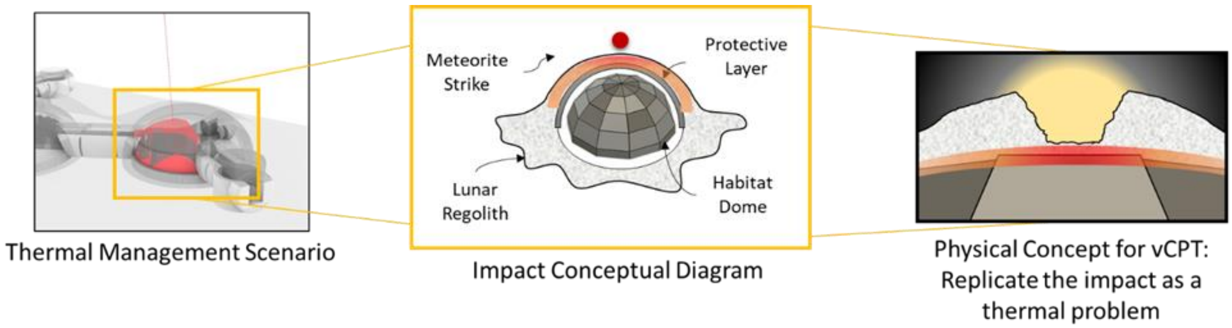


Figure 3. Impact scenario replicated in the physical environment as a thermal problem.

How this transition is carried out is further illustrated in Figure 4. In the virtual simulated environment, the SPL receives a meteorite impact at a specified location. The consequence of the numerical calculation is subjected to be transferred as the interface boundary condition to the physical structural thermal system. The thermal transfer panels at the node junction connecting the virtual and physical substructures (*i.e.*, interface between SPL and Structural System) will enforce the appropriate interface condition, surface temperature. This prompts the simulation data to be translated to cascading physical effects, initially starting from the structural system and to interior environment. Then, these physical responses are captured by the respective sensors and used as feedback for the virtual environment, numerical models to complete a loop for one simulation timestep.

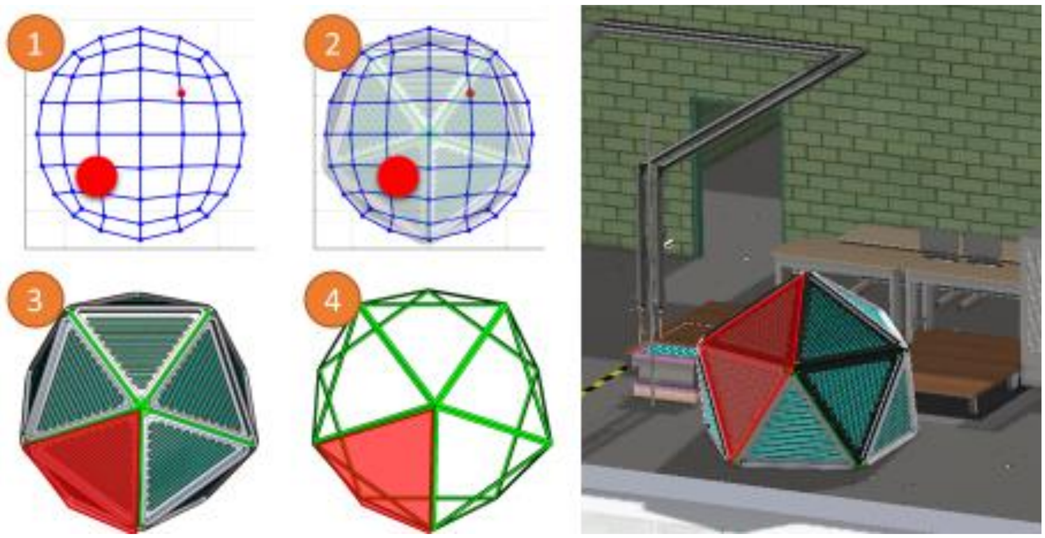


Figure 4. Impact scenario example with cascading effect originating from cyber substructure to physical substructure.

### 2.1.1 MCVT Example: ECLSS and Interior Environment

By a way of illustration to better display the MCVT framework and its practical use case, a snapshot of the software user interface is provided in Figure 5. In addition, one result of a simple case study, conducted by using MCVT, is discussed in detail. In this case study scenario, only two full systems, ECLSS and the interior environment, were activated in MCVT, and other subsystems were disabled for benefit of simplicity. The primary disturbance to the system was chosen to be the inner wall temperature of the interior environment, whose behavior was described as a combination of step functions. In the version of MCVT, used for the case study, the interior environment was represented as a lumped air model with the assumption of ideal gas which exchanges heat with wall surfaces via natural convection, and ECLSS was modelled to have a two-phase refrigeration cycle and a simple resistive electrical heater for cooling and heating, respectively [25]. Model functionalities of these two models are described in Table 2.

Table 2. Summary of functionality description for ECLSS and interior environment

| Subsystem Model | Functionality Description |
|---|---|
| **ECLSS** | Provides appropriate heating or cooling loads to the interior environment to maintain the desired setpoint temperature.<br>Captures the dynamic of heating and cooling systems as electrical heater and refrigeration cycle respectively |
| **Interior Environment** | Captures the coupled dynamics of pressure and temperature of air bound by the structural system.<br>Takes inputs from ECLSS as heating or cooling loads, and from structural system as wall surface temperature. |

The purpose of this case study was to evaluate the behavior of lumped temperature and pressure values of the interior environment in response to the changes in wall temperature and control measures taken by the temperature control system in ECLSS with progress in time. For the scenario, a simple virtual PI controller was implemented to control the cooling and heating subcomponents of ECLSS with the temperature setpoint of 25 °C. As shown in Figure 6, the inner wall temperature stays the same as the initial temperature of the interior environment, at time 500 seconds and 1000 seconds, it drops to 0 °C and rises to 70 °C in “steps” respectively. Due to these disturbances, the pressure and temperature of the interior environment become affected. However, temperature control in ECLSS provides appropriate cooling and heating loads to quickly restore the temperature value of the air inside the habitat to the desired setpoint value of 25 °C. For this simple case study, only the partial interaction between the interior environment and ECLSS was activated. In practical usage, MCVT can host many subsystems and provide meaningful data for analyzing complex interdependencies of subsystems which constitute an extra-terrestrial habitat and its surroundings.

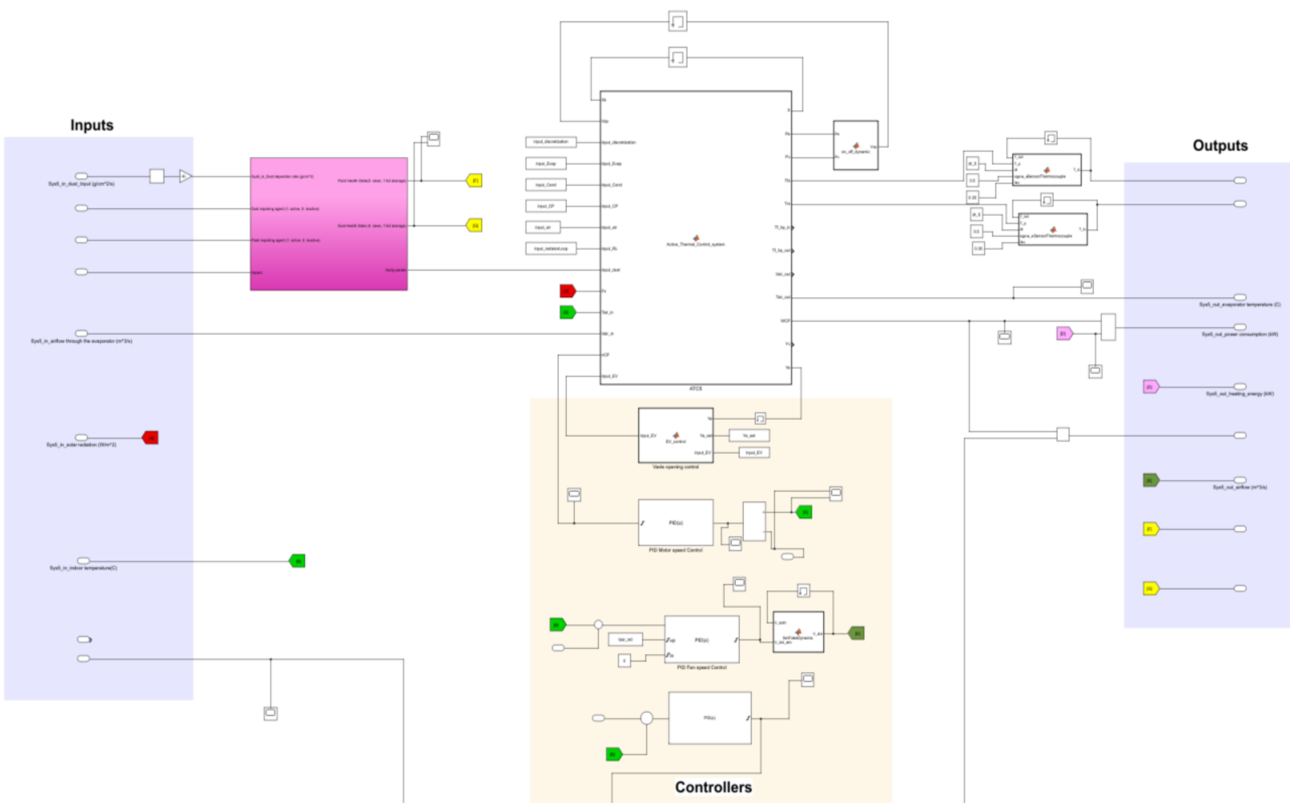


Figure 5. A snapshot of the Simulink environment displaying a section corresponding to the temperature control system of ECLSS.

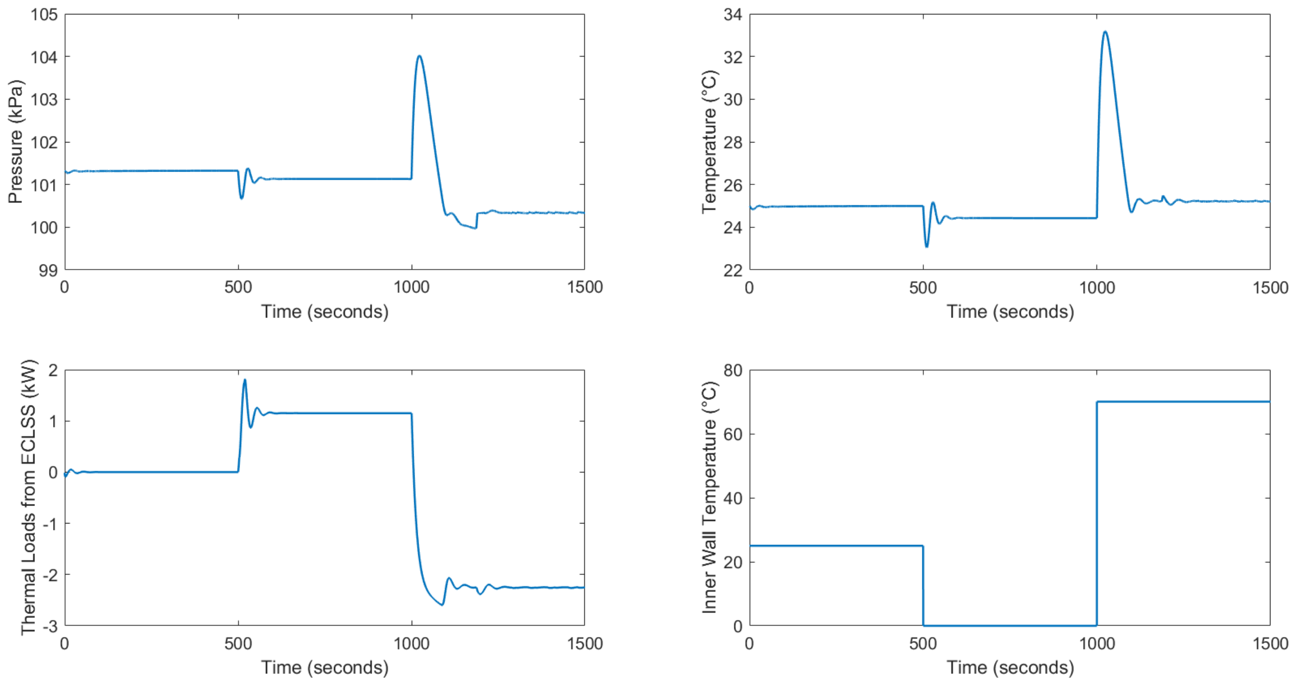


Figure 6. Sample scenario case results generated by the MCVT simulation platform.

### 2.2 Physical Substructure

As the physical substructure contains the main targets of in-depth investigation in the architecture of the CPT, the design of it should be carefully considered and planned. As shown in the previous sections, only handful of subsystems are chosen to be realized as the physical subsystems. Often, the choice was made based on process of elimination due to the lack of resources on earth. For example, Structural Protective Layer was not considered for physical realization as the lunar regolith was not readily available on earth. Similarly, the effect of microgravity was omitted for the interior environment and Structural Environment. The space constraints in the lab limited the size of the habitat, therefore limiting the entire CPT to be scaled down appropriately. On the other hand, subsystems which could be designed with more ease or did not require substantial amount of resource were proactively considered for physical realizations. Temperature and pressure control systems in ECLSS, for instance, could be designed with commercially available product, such as heat pumps, pressure regulators, and tubes, based on the interior environment load requirements. Likewise, Command and Control System, an interactive decision-making algorithm in the form of software, did not require actual physical resource other than high performance computers.

Design of physical interior environment and structural system has been an iterative process, which requires a close coordination among researchers from different field of specialties. Some parts of the design are still subject to changes, but the bodywork has been completed. As detailed walkthrough of the decision-making process with engineering analysis is beyond the scope of this section, a summary of design evolution in time is provided as illustrations in Figure 7. In each design iteration, thermal transfer panels were thought to be assembled at the outermost layer of the structural system. The performance requirements and design process for the transfer system will be discussed in depth in following sections. The first design takes the form of a half-dome with trapezoidal surfaces. Due to the issues with structural integrity and non-uniform panel faces, this design was no longer considered. As an alternative, a geodesic dome design was suggested. The second design included a bladder (yellow) and a layer of thermal interface material (purple) to accommodate pressure-related tests and improve heat transfer between the interior environment and thermal transfer system. The problem with many triangular faces and the manufacturability of the thermal transfer panels having to match the shapes encouraged the design to be further simplified. The third design, reducing the complexity of the geometry, still inherited the idea of using a bladder. Having a smaller number of triangular faces while keeping the faces uniform, the design significantly reduced the complexity of manufacturing and commissioning, especially for the thermal transfer system. This last design was selected for the production.

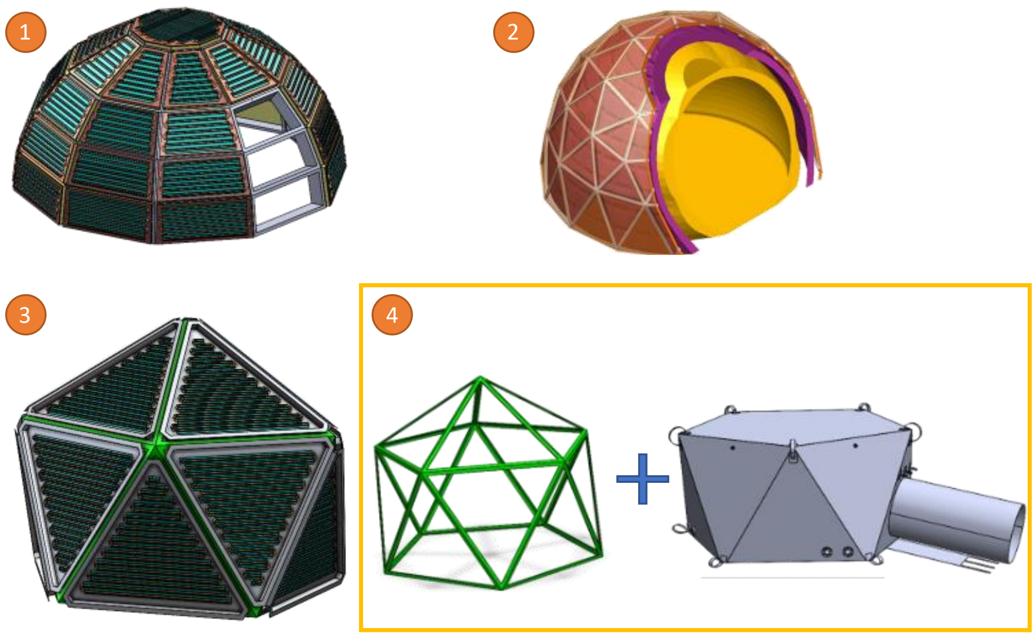


Figure 7. Design evolution of Interior Environment and Structural System

### 2.2.1 Thermal Management System

The active thermal control system is a subsystem of ECLSS in MCVT and its primary function is to maintain the desired interior environment temperature setpoint. Within CPT, the active thermal control system is to be constructed as a physical system that will interact with the cyber environment. Fundamentally, the physical thermal control system is responsible for providing appropriate cooling and heating to the interior environment to maintain its temperature close to the setpoint temperature necessary to ensure the safety and comfort of human crew members as well as the correct operation of equipment (*e.g.*, power electronics). Within the context of CPT, the physical realization of the thermal control system needs to be compatible with the current design of the interior environment and the range of thermally engaged disturbance scenarios. Therefore, a proper estimation of heating and cooling load is to be carried out, followed by a selection of components according to the estimated thermal loads. In addition, the thermal control system itself should feature a variety of simulated damageability to further expand the scope of potential simulation scenarios which can be tested. For example, one might be interested in investigating the impact of thermal control system malfunctioning on the interior environment (*e.g.*, air blower failure and thermostat malfunctioning). By having multiple, or even redundant, tune-able parameters, these types of scenarios can be readily reproduced without physically harming the system itself.

To conduct a thermal load estimation of the interior environment, a quasi-static thermodynamic analysis was performed based on a lumped-capacitance model [26]. It was assumed that the air inside the bladder was well-mixed and behaves as the real-gas air, whose thermodynamic properties were obtained from tabulated values within CoolProp Library [27]. Given the range of simulation scenarios and practical limitations of the cryogenic chiller and thermal transfer panels, interior wall temperature values between -50 °C and 70 °C were considered. The primary heat transfer phenomenon was assumed to be natural convection. The convection heat transfer coefficient was obtained by using the correlation for vertical walls [28],

$$\overline{Nu}_L = \left\{0.825 + \frac{0.387 Ra_L^{1/6}}{[1 + (0.492/Pr)^{9/16}]^{8/27}}\right\}^2 \tag{1}$$

where $\overline{Nu}_L$ is the Nusselt number, $Pr$ is the Prandtl number, and $Ra$ is the Rayleigh's number. The geometry of the interior environment, the bladder, was treated as an equivalent cylinder whose top and bottom surfaces were insulated. The desired setpoint temperature for the interior air was kept at 25 °C. The resulting heat transfer rate between the air and interior wall would be then the estimated heating or cooling load to be supplied by the thermal control system to maintain the temperature. Table 3 provides a summary of parameters used for the estimation of loads.

Table 3. Parameters used for thermal load estimation

| | | | |
|---|---|---|---|
| **Area of top and bottom surfaces** | 6.15 $m^2$ | **Temperature of insulation pad** | 23 °C |
| **Area of lateral surface** | 10.49 $m^2$ | **Interior wall temperature** | -50 °C ~ 70 °C |
| **Air volume** | 7.34 $m^3$ | **Interior air temperature** | 25 °C |

Figure 8 shows the result of the estimation. Both heating and cooling loads are expressed in terms of their magnitude in Watts. Estimation of heating load is indicated to the left of 25 °C mark on the horizontal axis, and estimation of cooling load is indicated on the right. It is clear the heating load requirements are larger than the cooling load requirements. The maximum requirements are approximately 6.6 kW and 2.8 kW for heating and cooling respectively. Therefore, with respect to the sizing of the thermal control system, the architecture design is conducted to achieve 2-RT (refrigeration tons) capacity.

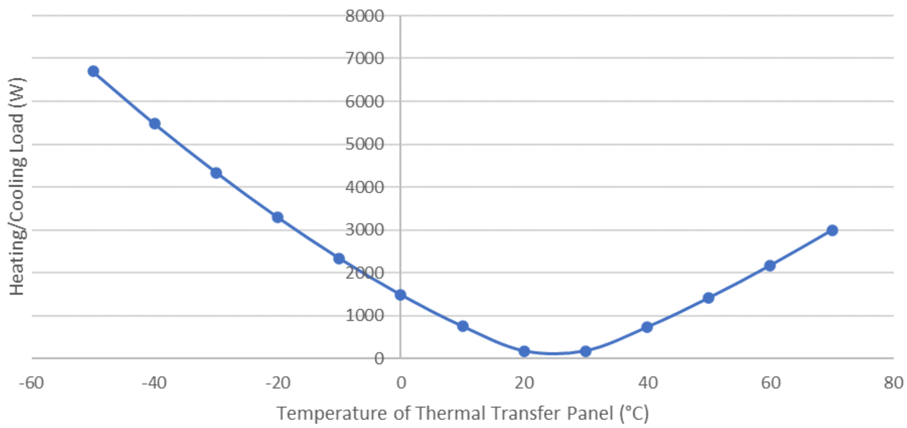


Figure 8. Estimated cooling and heating load required by thermal control system

After a careful consideration of load requirements and scenario-related functionalities, the thermal control system architecture is developed as shown in Figure 9. For the outermost loop, a commercially available, air-to-liquid heat pump system is selected to heat or cool the secondary water loop. The secondary water loop is essentially a water-glycol, single-phase loop which is driven by a variable-speed pump. The water-glycol mixture is then fed into the air-liquid coil heat exchanger situated inside the bladder to control the temperature of the interior air. Overall, there are mainly three tune-able control parameters. Liquid temperature setpoint can be adjusted from the heat pump, the flowrate of the water-glycol mixture can be controlled by the pump, and air speed in the interior environment can be regulated by the fan control. These parameters are to be controlled in real time by a testbed computer. Having the controllers all collocated on one computer allows the physical thermal control system to communicate with the rest of subsystems which reside in cyber platform. Having multiple layers of controllability yields more freedom in designing the test scenarios and consequently makes CPT more versatile.

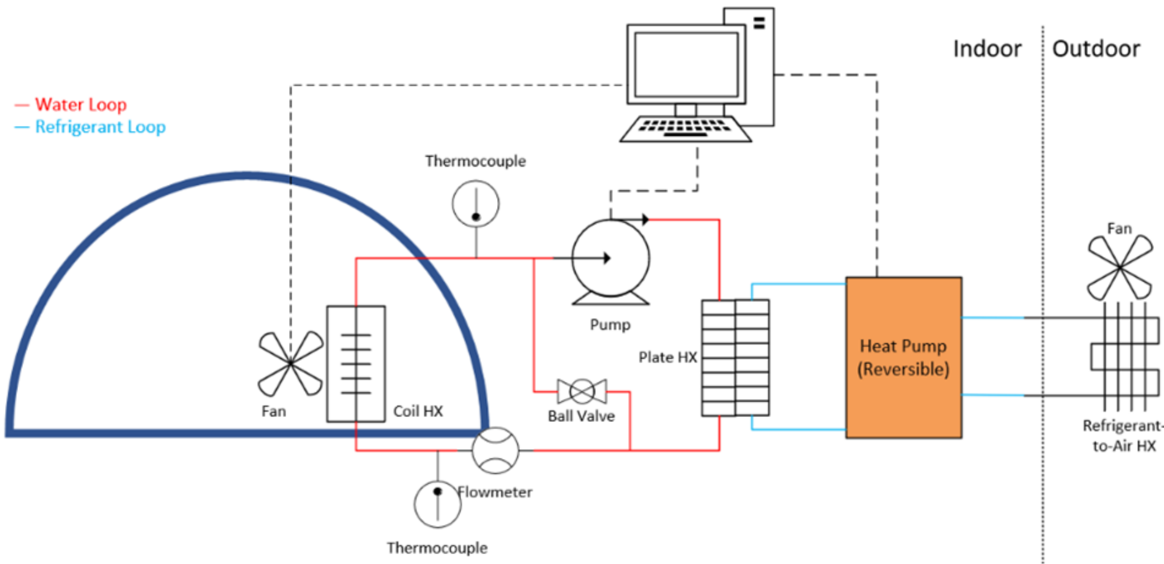


Figure 9. Thermal control system architecture

Depending on the assumptions and modeling approach of the interior environment, the estimate of the required heating and cooling load calculations may vary. For simplicity, it is assumed in the above that the influence of both the movement of ventilating air and of radiation is minimal during the analysis above. This assumption leads in the model in which the natural convection is the dominant mode of heat transfer, where the heat transfer coefficient for natural convection is mainly a function of the interior air and wall temperatures. Figure 10 shows the range of calculated heat transfer coefficients used for the load estimation. The coefficient can take values between 3 W/m$^2$-K and 9 W/m$^2$-K. For more detailed modeling, one might relax the assumptions and incorporate the impact of forced convection and radiation. With regards to the lump-capacitance modeling approach, Table 4 briefly summarizes the margins of heat transfer coefficient values. As the current interior environment is comparable to automobile cabin for its size, coefficient values used for cabin modeling were also reviewed in addition to the those used for house modeling. The reported values for the heat transfer coefficient do not deviate much from the range of values used in load estimation by natural convection only. It is also possible to use computational fluid dynamics (CFD) software to conduct a high-fidelity estimation. However, this level of detail was considered unnecessary as the primary purpose of the analysis was to establish the basis for sizing and selection of the components of thermal management system.

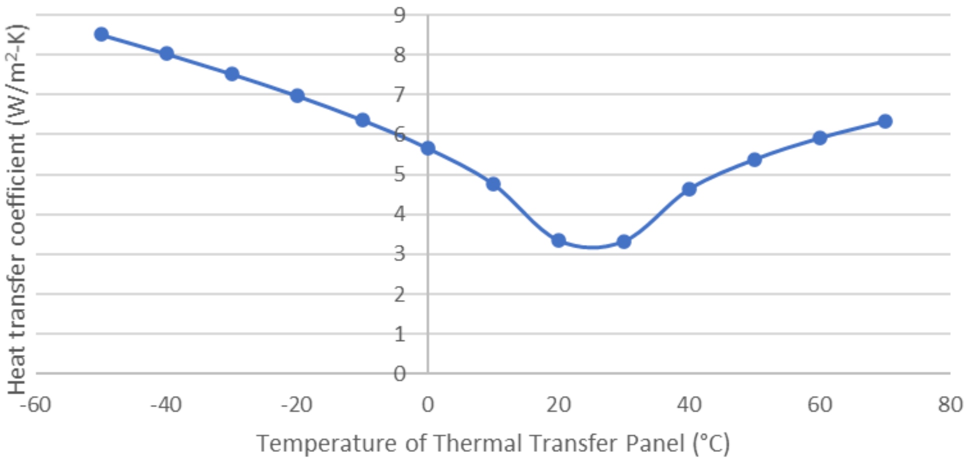


Figure 10. Heat transfer coefficient on various wall temperatures

Table 4. Literature reported values for convection coefficient for lumped capacitance modeling

| **Modeling Type** | **Value** | **Source** |
|---|---|---|
| House | 2-6 $W/m^2$-K | [29] |
| House | 0.35-2.465 $W/m^2$-K | [30] |
| House | 9.825 $W/m^2$-K | [31] |
| Automobile cabin | 4.4 $W/m^2$-K | [32] |
| Automobile cabin | 4.65 $W/m^2$-K | [33] |

### 2.2.2 Pressure Management System

As another component of ECLSS, the interior pressure control system manages the pressure inside the habitat to ensure the safe operation of the crew members and equipment by maintaining the desired setpoint pressure. The importance of the pressure management is especially spotlighted in case of leakage or over-pressurization of the habitat. As briefly described in previous sections, a simulation case scenario can include a perforation of the habitat structure by the meteorite impact, which initiates air leakage from the interior of the habitat to the vacuum of the space outside due to significant pressure gradient. It is then up to the pressure management system to provide adequate supply of air to compensate for the leakage and hold up the system until proper repair or evacuation has taken place. Conversely, intentional release of air from the habitat can be beneficial when the habitat is introduced to a surge of pressure (*e.g.*, oxygen line valve stuck open) or in case of extinguishing fire in a compartment by blocking oxygen.

In relation to the actual CPT, the architecture for the interior pressure control system is created as illustrated in Figure 11. The architecture consists of main two loops, which are for supply and relief respectively. The supply line uses a pre-existing pressurized line in the lab as a reservoir. This pressurized channel can take pressure between 150 PSI and 75 PSI, depending on the load from other users in the lab, the lower bound, 75 PSI, is assumed as the minimum available reservoir pressure for the sizing calculations. Practically, a manual regulator with a moisture filter (dryer) sets the upstream pressure to be always less than 75 PSI, while also limiting the moisture content in the air. Then, there is another pressure regulator, which can be controlled electronically. The electronic regulator is a representation of the supply air tank whose pressure can increase or decrease in the course of simulation. Therefore, it can be also viewed as a simple transfer system which takes the result of pressurized air tank model and reproduce it as a physical realization. To fine control the flow rate of the supply air, an actuated valve is installed to be also controlled electronically. On the other hand, the relief line is solely controlled by an actuated valve. The bladder is pressurized 8 PSI above the outside atmospheric pressure to emulate the magnitude of the pressure gradient that would exist between the extra-terrestrial habitat and the deep space environment. The relief line essentially utilizes this pressure gradient to naturally give rise to the flow of air from the inside to the outside of the bladder.

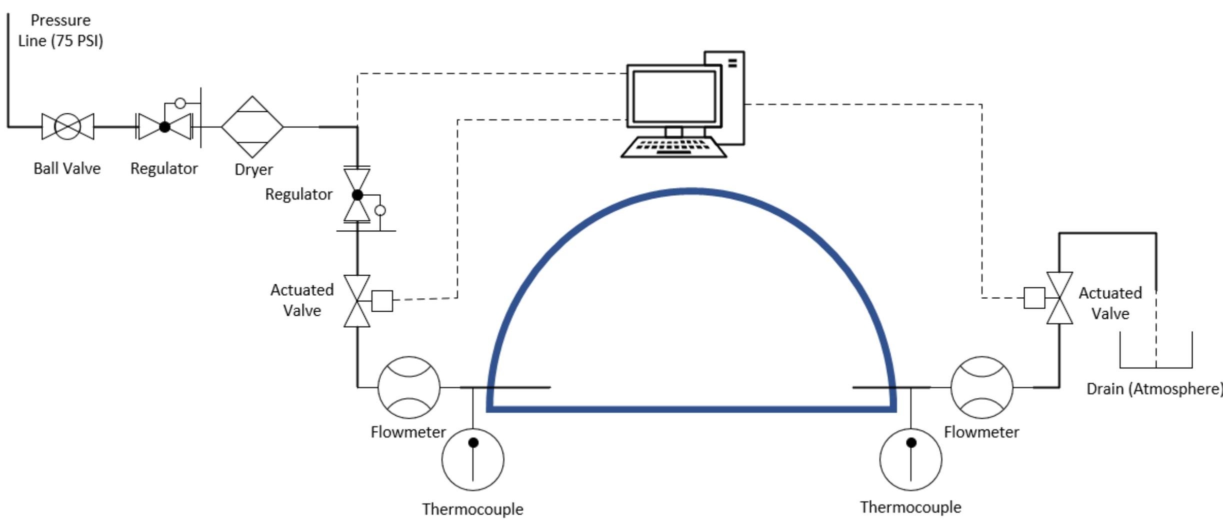


Figure 11. Interior pressure control system architecture

To test the plausibility of the architecture, especially concerning the usage of pre-existing pressure line in the lab, a basic sizing estimation was conducted. As the first step for this procedure, the mass flow rate of the air due to the leakage was predicted. For the current design of the bladder, it features ¼ inch threaded connection to function as a port to mimic the perforation which can happen on the structural part of the habitat. The severity of the leakage would be then dependent upon the valve opening position. For this sizing calculation, it was assumed that the valve is fully opened, and the area of the port is the area of the hole due to damage of the structure. Using the conventional modeling approach for orifice flow [34], the formulation

$$\dot{m}_{leak} = KA_t\sqrt{2\rho(p_1 - p_2)} \tag{2}$$

was used to estimate the mass flow rate of the leak, where $K$ is the discharge coefficient, $A_t$ is the cross-sectional area for the hole, $\rho$ is the density of air, and $p$ is the pressure of the air inside and outside of the bladder. The resulting leakage mass flow rate was calculated to be about 0.008 kg/s, which is about 10 CFM at standard air conditions. Then, the calculated flow rate was used to estimate pressure difference required for the supply line by taking the theoretical formulations presented in [35]

$$\Delta p = \lambda \frac{8L\rho_N Q_N^2}{\pi^2 D^5} \frac{T}{T_N} \frac{P_N}{P_1} \tag{3}$$

where $L$ is the length of the tubing, $Q$ is the volumetric flow rate, $D$ is the diameter of the tube, and $T$ is the temperature. Moreover, subscript $N$ refers to the thermodynamic properties at standard conditions, and $P_1$ refers to the upstream pressure. The friction coefficient, $\lambda$, is obtained by

$$\lambda = 0.3164(Re)^{-\frac{1}{4}} \tag{4}$$

where $Re$ is the Reynolds number for the flow, which can be expressed as:

$$Re = \frac{4\,\rho_N\,Q_N}{\pi\,D\,\mu} \tag{5}$$

where $\mu$ is the dynamic viscosity of the air. Table 5 presents the parameters used or assumed for the calculation. The pressure drop required across the supply line was calculated to be about 33 PSI, which results in requiring the upstream pressure to be 56 PSI. As the required upstream pressure is lower than the minimum reservoir pressure of 75 PSI, it was concluded that the current design of the pressure control system architecture would meet the requirement (i.e., it is able to fully compensate for the leakage).

Table 5. Parameters used for sizing of the supply pressure line

| | | | |
|---|---|---|---|
| **Diameter of leakage hole** | ¼ in | **Downstream (bladder interior) pressure** | 23 PSI |
| **Diameter of air tube** | ¼ in | **Outside air pressure** | 14.7 PSI |
| **Air temperature** | 25 °C | **Discharge coefficient** | 0.5959 |
| **Length of tube** | 10 m | | |

## 2.3 Transfer System Substructure

Thermal transfer system functions as a bridge between physical (*e.g.,* dome structure) and virtual components (*e.g.,* impact scenarios, case studies) of the cyber-physical testbed. Within the context of modeling a future extraterrestrial habitat, the thermal transfer system emulates the interface between Structural Protective Layer (SPL) and Structural System (SS). It provides accurate and responsive thermal boundary conditions to the physical habitat structure. Practically, it is built as an attachment, in the form of heat transfer panels consisting of pipes and heat-spreader plates, to the structural dome which is the portrayal of the lunar habitat. Figure 12 summarizes the layout of the Cyber-Physical Testbed (CPT) by grouping sub-components into three substructures: cyber, transfer, and physical. Depending on the case study, there can be more than one type of transfer system. Figure 12 shows two additional transfer systems for handling structural mechanical and pneumatic problems. Such transfer systems are to be considered and planned to be added to the overall architecture of CPT. However, for the scope of this section, only the thermal transfer system is discussed in depth.

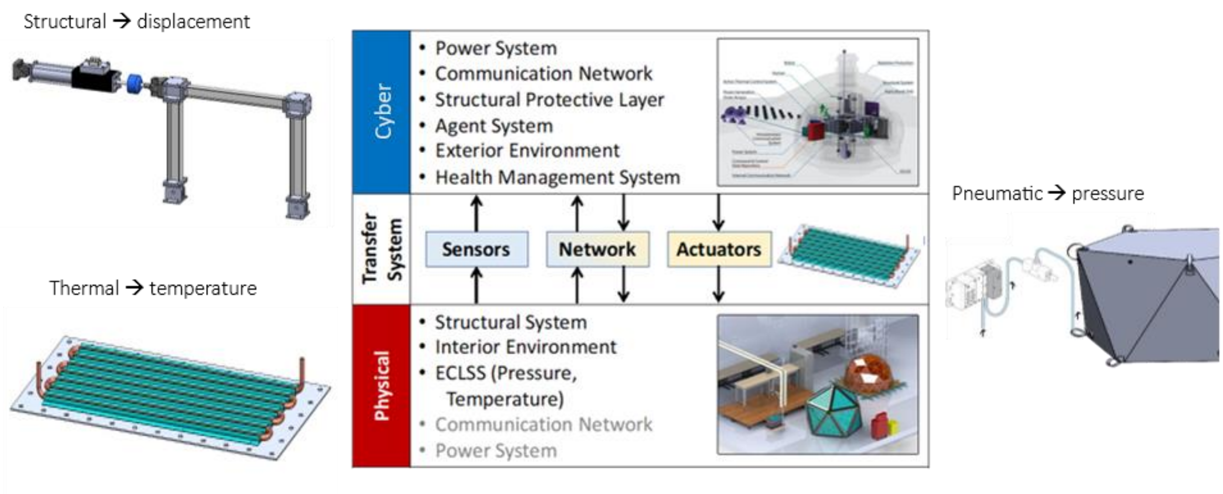


Figure 12. Division of CPT into cyber, transfer, and physical substructures and examples of different types of transfer systems

### 2.3.1 Thermal Transfer System Architecture

The thermal transfer system achieves the coupling between cyber and physical substructures by forming a feedback loop involving temperature and heat flux. Figure 13 presents such feedback loop with labeled signals. First, external disturbances such as meteorite strike or solar irradiation are recreated in numerical simulation, with the help of MCVT in MATLAB/Simulink environment according to user inputs. These disturbances will affect the behavior of SPL, the physical, outermost part of the habitat. Then, the interface temperature at the contact junction between SPL and SS is calculated by MCVT as a result of the cascading effects of external disturbances. Through the secondary control loop between the cryogenic chiller and the thermal transfer panel, the calculated interface temperature from the cyber substructure is physically reproduced. The physical coupling between the SS and the thermal transfer system allows heat transfer, in both directions, to take place at the contact surface. As a result, the thermal transfer system is affected in a way that can be deduced from the temperature measurement by a form of heat flux. At the interface between the thermal transfer system and the face of SS, there can be multiple temperature measurements taken. These temperatures can be used to get meaningful information regarding the heat flux quantity at the contact surface. The exact method of obtaining the flux estimate requires further investigation at the current stage of development. To complete the feedback loop, this information is then returned to the cyber substructure, which uses it to solve the systems of differential equations for the next discrete timestep.

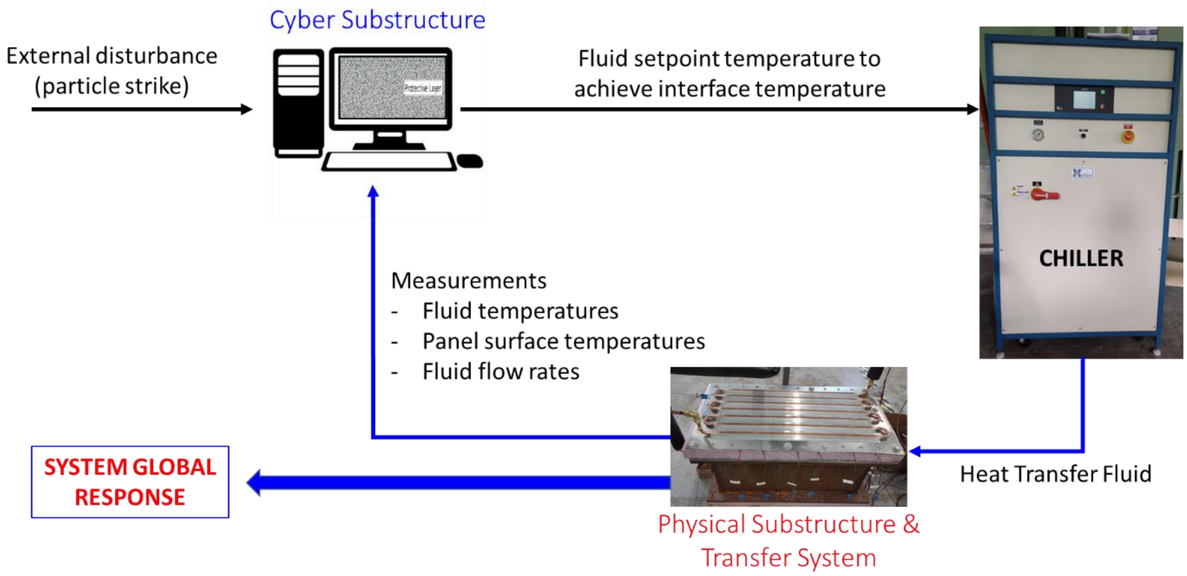


Figure 13. Schematic of the thermal transfer system architecture

To illustrate an example of how a disturbance scenario can be simulated involving thermally driven dynamics, Figure 14 is presented. According to the result of cyber substructure simulations, impact magnitude and location are decided. For the current setup of the thermal transfer panels and their couplings to SS, the temperature will represent the magnitude of the disturbance, and individual panel will correspond to the location of the disturbance. The thermal boundary condition is then physically realized as a form of contact surface temperature between the thermal transfer panels and SS. The effect of this thermal disturbance will cascade through the thickness of SS and reach the interior of the habitat, also defined interior environment (IE). The cascading effect is likely to cause interior air temperature to deviate from the setpoint temperature, thus triggering control action by physical, temperature control system. As a part of ECLSS, the temperature control system may or may not be able to restore the physical states of the interior environment depending on case scenario which can have a range of variations in severity of the disturbance.

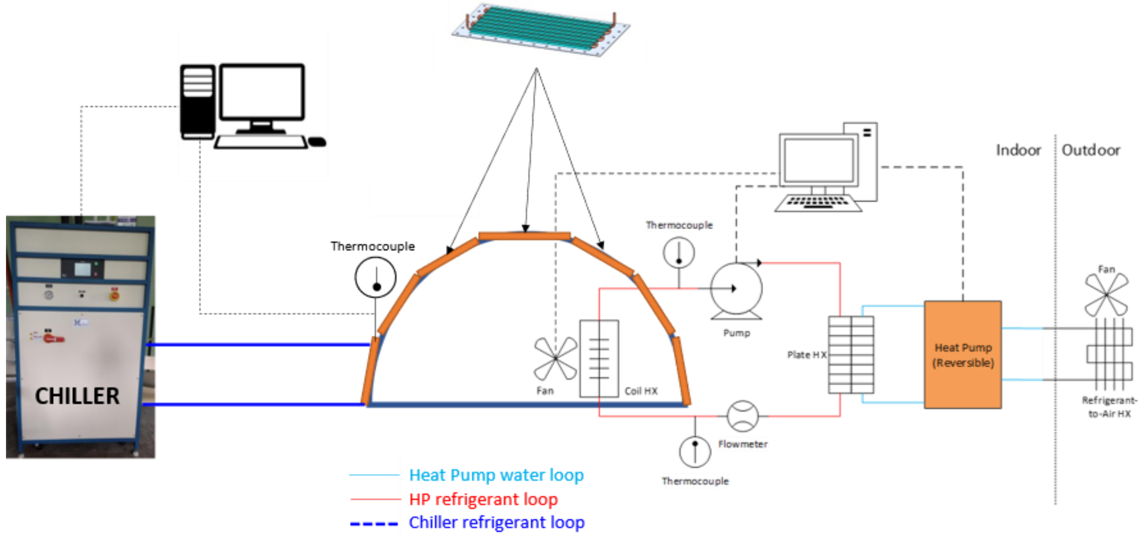


Figure 14. Thermal case study scenario and temperature management architecture

Based on the proposed design of the structural system, general shapes and dimensions of heat transfer panels are determined and modified to ensure the compatibility of the assembly. Figure 15 shows the two thermal transfer panels that are being developed and tested. The rectangular panel on the left has been designed and fabricated based on the previous geometries of the structural system and interior environment. The fabricated panel is used for a performance mapping of the chiller and small-scale testing, discussed in following sections in detail. Based on the useful data acquired and lessons learned during the physical prototype testing involving the rectangular thermal transfer panel, the design is to be improved and adjusted to increase compatibility with the current design plan of the CPT setup, therefore having a triangular face as shown in the right side of Figure 15.

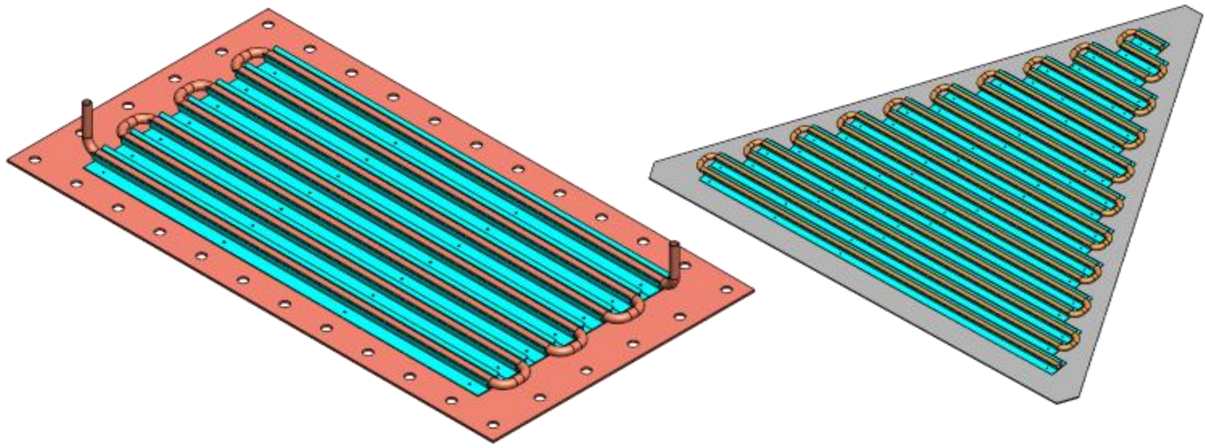

Figure 15. Prototype designs thermal transfer system for pressure box testing (left) and for full-sized CPT setup (right)

One of the main driving factors of the capacity for the current thermal transfer panel is the temperature of the fluid which travels through the pipes. As the heat transfer fluid needs to support a wide range of scenarios that the thermal transfer system needs to emulate (*e.g.*, extreme temperatures of lunar regolith during day and night), a dedicated cryogenic chiller has been selected to cover a wide range of the desired boundary condition requirements while being mindful of current constraints of the laboratory environment. Table 6 summarizes the specification of the cryogenic chiller shown in Figure 16. Although the chiller does not cover the entire range of lunar surface temperature between 120 K and 374 K as suggested in [36], the fluid temperature difference of 150 °C gives a sufficient room for variety of simulation scenarios to be tested. In practice, multiple thermal transfer panels will form a pipe network of both serial and parallel connections to ensure proper distribution of the fluids within the allowed capacity of the pump.

Table 6. CryoDax 16 cryogenic chiller specification

| **Recirculating Fluid** | Syltherm XLT | **Net Cooling Capacity** | **Fluid Operating Temperature** |
|---|---|---|---|
| **Fluid Temperature Range** | -70 °C to + 80 °C | 8 kW | -40 °C |
| **Temperature Stability** | ± 1 °C or better | 4.7 kW | -50 °C |
| **Heating Capacity** | 3 kW (230 VAC) | 2.2 kW | -60 °C |


Figure 16. Thermal transfer panel prototype and CryoDax 16 chiller

The current research focus is on the thermally driven case scenarios, but the investigation can be expanded into structural mechanical or pressure-related scenarios in the future. Therefore, it will be a natural progression for CPT setup to include more types of transfer systems other than thermal one. Such transfer system was briefly discussed in the previous section as the electronically controllable pressure regulator serving as a proxy for the pressurized oxygen tank. With the similar logic, control valves on the bladder can be also considered as crude transfer systems which represent simulated disturbances involving a perforation, therefore an air leakage, of the interior environment.

# 3. PROTOTYPE TESTING

## 3.1 Development of Thermal Transfer Panel

Thermal transfer system is used to enforce thermal boundary conditions at the interface between Structural System (physical) and Structural Protective Layer (cyber) in the form of contact surface temperature. To the end, heat exchangers involving solid surfaces, therefore conduction as one of heat transfer phenomena, were reviewed. Due to the simplicity of the design and applicability in both heating and cooling situations, a “traditional cooling plate” [37] design was selected for further evaluation and customization. Operating on the concept of conjugate heat transfer, involving both convection and conduction, the cooling plate, also called a cold plate, design has proven its versatility in wide range of applications ranging from electronics cooling [38] and solar collectors [39], and even to the heat rejection for Active Thermal Control Systems in Lunar and Martian habitats [40].

The basic design usually involves a flat plate and fluid channels which are either straight or serpentine-like as shown in Figure 17. To facilitate the heat transfer between the circular pipes and flat plate, heat spreaders were added in between. Copper was chosen for the material of the pipes, and aluminum was selected for the plate material. For the setup of CPT, copper pipelines of such thermal transfer panel will provide the pathways for the heat transfer fluid from the chiller to travel. The flat plate side will be in contact with the outermost layer of the structural system, which is the outer surface of the bladder holding pressurized air. Depending on the temperature of the fluid in the pipes, the thermal transfer panels can provide both heating and cooling to the structural system in contact.

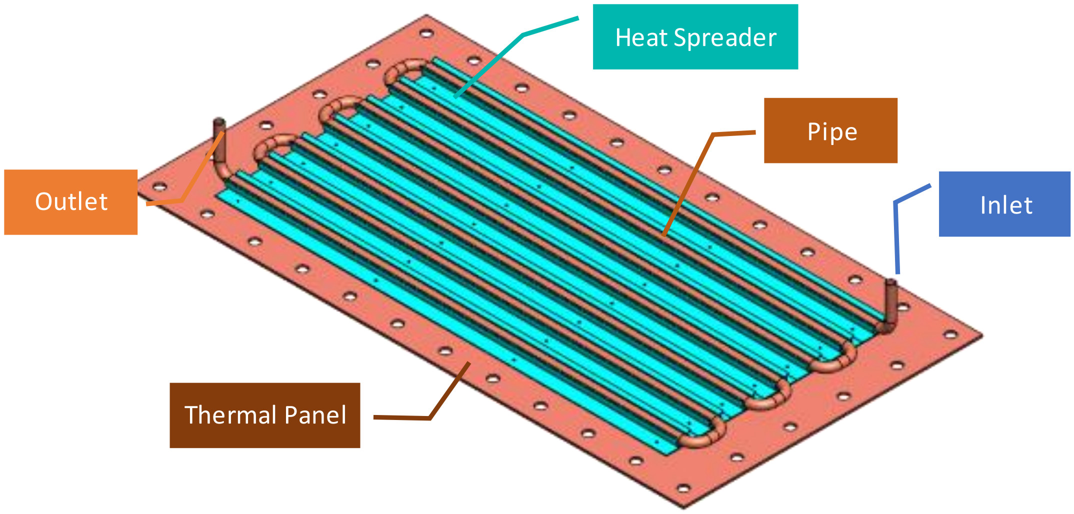


Figure 17. “Cold plate” design adaptation for thermal transfer system of CPT setup

Various efforts for optimization were made for the prototype design to be finalized as shown in Figure 17 based on three main criteria: average plate surface temperature, surface temperature uniformity, and pressure drop through the pipes. Having a plate surface temperature closer to the inlet heat transfer fluid temperature would indicate that there is an effective heat transfer between the solid plate and the heat transfer fluid and mean that wider portion of the chiller operation range is reflected by the resulting plate temperature. Uniform temperature profile of the panel would allow a simpler modelling approach to be taken for the numerical part of the feedback loop and can reduce the number of thermocouples used to monitor the plate temperature during testing. Minimizing the pressure drop through the pipes would alleviate the global constraint imposed by the capacity of the chiller pump so that greater number of pipe network configurations could be considered among multiple thermal transfer panels to better accommodate the types of simulation scenarios.

Parametric studies of pipe geometry were conducted using computational fluid dynamics simulation (CFD) software, primarily by SolidWorks Flow Simulation Add-on whose results were later cross verified with Ansys Fluent. The varying parameter were the number of loops, therefore the distance between them, on the cold plate and the flow rate value of the running heat transfer fluid. Pipe head losses through the pipes were also estimated for each of parametric study setting. Design parameters and material properties used for the parametric studies are summarized in Table

7. Total four configurations of the pipe layout, four, five, seven, and nine loops, were considered and five flow rates evenly spaced out from 0.4 to 1 GPM were chosen for the investigation. The inlet heat transfer fluid temperature was held at -60 °C, which was within the specification of the cryogenic chiller discussed previously. Plate material was set to be copper.

Table 7. Parameters used for CFD simulations and pressure drop calculations

| | | | |
|---|---|---|---|
| **Convective Heat Transfer Coefficient** | 10 W/m-K | **Minor Loss Coefficient (180 Degree Elbow)** | 0.2 |
| **Ambient Temperature** | 25 °C | **Minor Loss Coefficient (90 Degree Elbow)** | 0.3 |
| **Heat Transfer Fluid Density @ -60 °C** | 937.4 kg/m$^3$ | **Pipe Surface Roughness** | 0.0015E-3 m |
| **Heat Transfer Fluid Viscosity @ -60 °C** | 9.4E-3 Pa-s | **Pipe Length (One Pass)** | 0.655 m |
| **Pipe Diameter (inside)** | 0.436 in | **Plate Thickness** | 1/8 in |

As illustrated in the left plot of Figure 18, the average panel temperature is closer to the inlet fluid temperature of -60 °C as the flow rate of the heat transfer fluid increases. The pipe configurations with more loops will result in the lower average panel temperature. However, it can be observed that at higher flow rates, there is less gain in performance between 9-loops and 7-loops configurations. A similar trend can be noted for the panel temperature range in the right plot of Figure 18. Here, temperature difference is calculated by subtracting the minimum temperature value of the panel from the maximum temperature. This value serves as an indicator for the temperature profile uniformity of the panel. Higher flow rates and more pipe loops allow the panel to have a more uniform temperature profile. In accordance with what is observed for the average panel temperature, increasing the number of loops from seven to nine does not make considerable difference in improving the surface temperature uniformity.

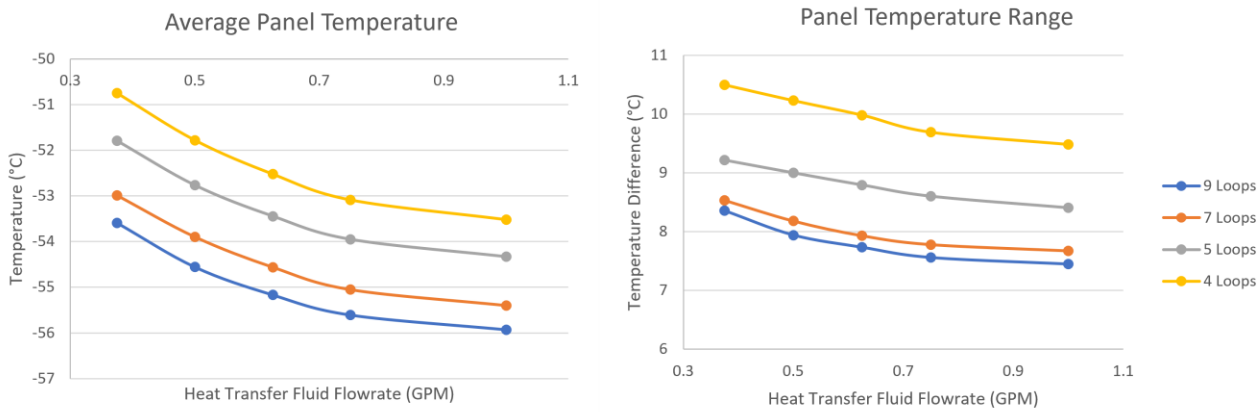


Figure 18. Average temperature and range of temperature in thermal transfer panel on various pipe loops and heat transfer flow rates estimated by CFD software (SolidWorks Flow Simulation [41])

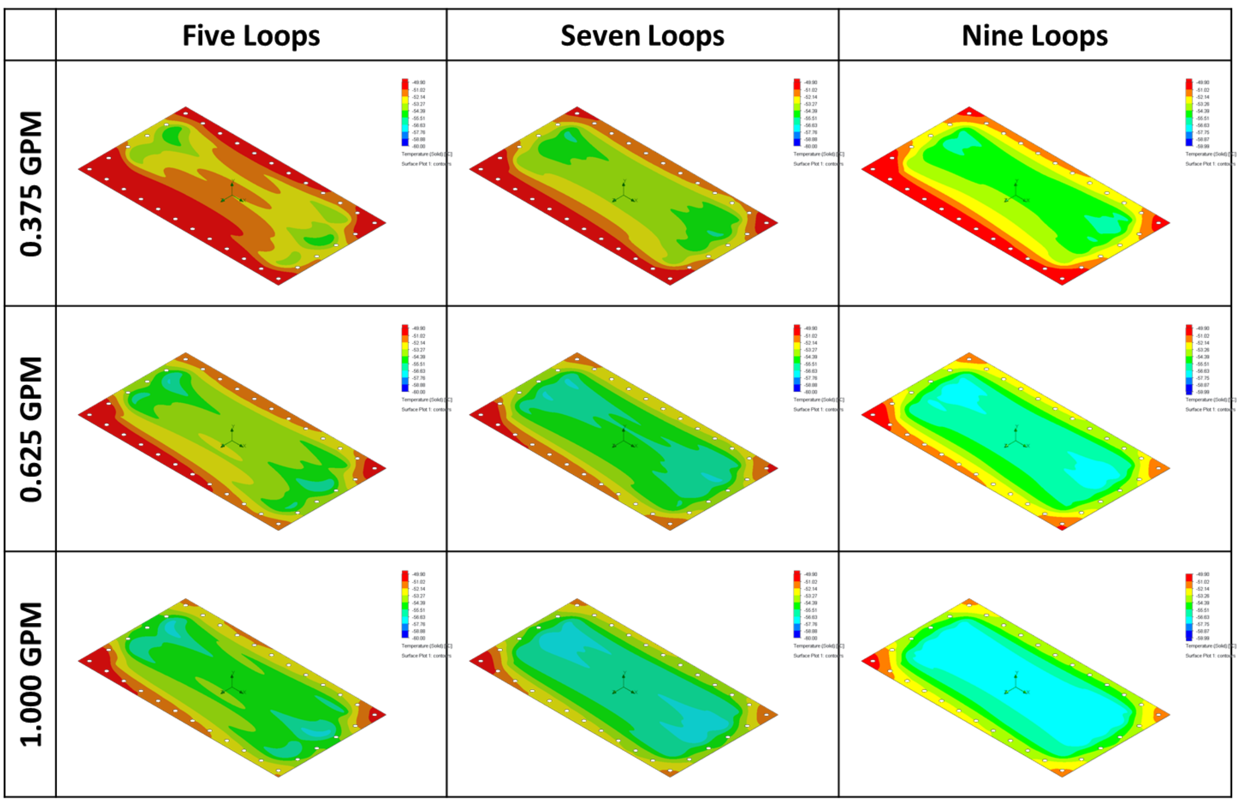


Figure 19. Sample results of parametric study showing temperature distribution across the panel surface

Pressure drop estimations across the pipes are presented in Figure 20. With the same inputs to the parametric study mentioned above, the head loss estimation suggests that pressure drop increases as the flow rate and the number of pipe loops increases. Within the relatively narrow region of interest for the heat transfer flow rate, the increase in pressure drop is rather gradual. However, there is a noticeable jump in the rate of increase depending on pipe configurations. The effect is the most pronounced when the number of pipe loops is increased from seven to nine. Based on these observations, the pipe layout involving seven loops was chosen as it would be providing comparable performance as the one with nine loops when the heat transfer fluid is at higher flow rate. The head loss saved by the decision will allow more flexibility in designing the pipe network of heat transfer fluid distribution system.

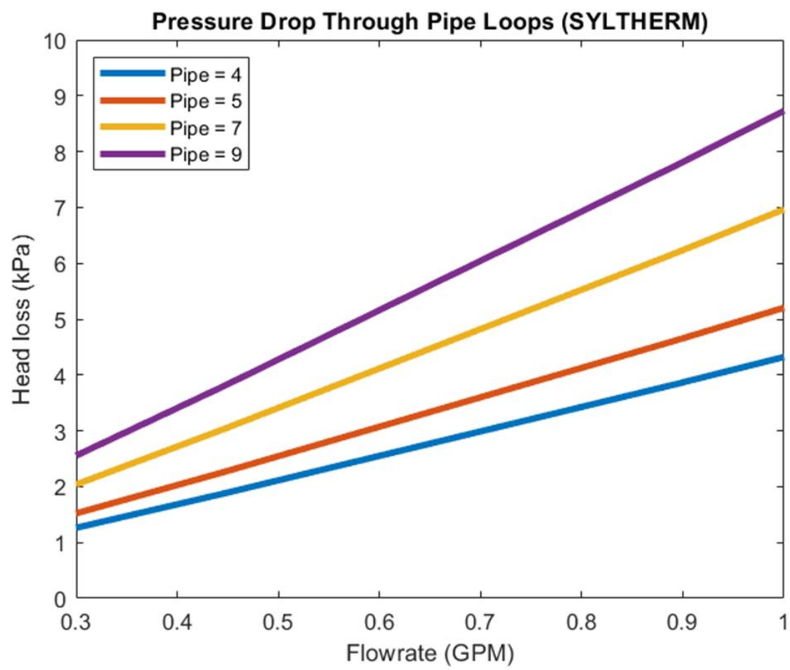


Figure 20. Pressure drops through the pipes on various pipe loops and flow rates

### 3.2 Performance Mapping of Prototype Panel

Through the design process of the structural system, concerns were raised that the forces exerted on the structural beams by the weight of thermal transfer panels might cause a permanent damage to the structure and create unsafe situations during testing. Even though copper has a very high thermal conductivity, it is very dense. Aluminum, which is almost three times lighter than copper for the same volume, was suggested as an alternative material for the plate. Therefore, it was necessary to investigate further whether there would be a sufficient justification to approve this change. To finalize the thermal transfer panel design and partially validate the calculation and simulation results, an experimental setup was contrived to test two versions of the cold plate designs, copper and aluminum plates, shown in Figure 21.

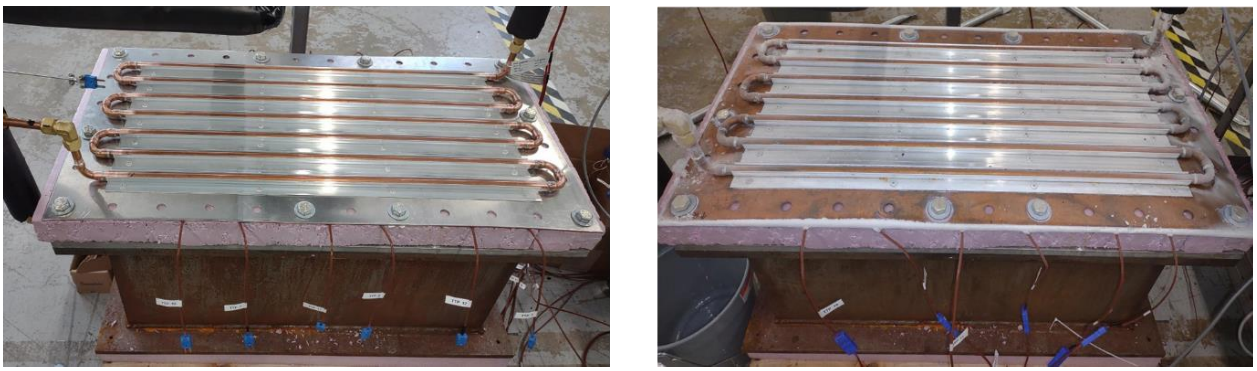

Figure 21. Two versions of prototype panels: aluminum plate (left) and copper plate (right)

Figure 22 describes the setup in pipe diagram with pictures. The experimental setup includes one heat transfer panel with single inlet and outlet pipe layout. It is connected to a chiller which circulates Syltherm XLT, silicone-based heat transfer fluid. A control valve with an actuator regulates the fluid flow, followed by a turbine flow meter which measures the volumetric flow rate of the fluid. To make fine adjustments to the fluid inlet temperature, a heating strip is attached to the pipe after the flowmeter. There is a total of 16 thermocouples installed for the test setup. Four of these thermocouples are used for fluid temperature measurements at the inlet and outlet of main supply channel and those of panel pipe channel. Rest of the thermocouples are used for capturing the surface temperature profile of the panel. The placement of these thermocouples is illustrated in Figure 23. Insulation layers are added both to the bottom and top surfaces of the panels. The result of this prototype panel testing is to be analyzed to make a final decision on the material of the heat transfer plate, either copper or aluminum, to obtain dynamic characteristics of the cold plate at sudden change of fluid setpoint temperature, and to map out the plate surface temperature distribution at various setpoint temperature of the heat transfer fluid. The sensors and hardware used for the testing is listed in Table 8.

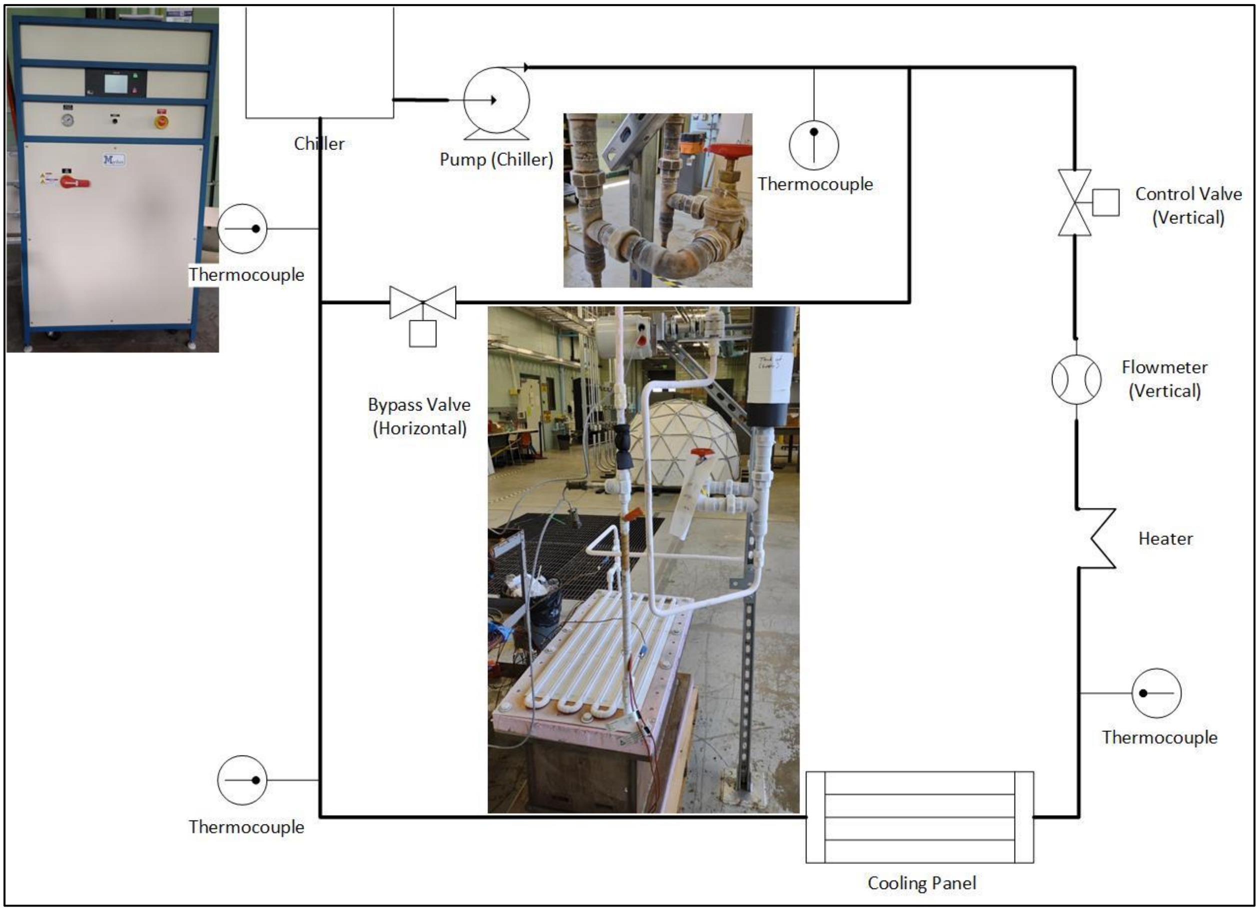


Figure 22. Pipe diagram for the single panel experiment setup

Table 8. List of sensors and hardware used

| Equipment | Manufacturer | Model |
|---|---|---|
| Thermocouple | Industrial Process and Sensor<br>Omega (Feedthroughs) | T-20-TT<br>PFT2NPT-4T |
| Thermocouple probe | Industrial Process and Sensor | TG20T0142U00600MP |
| Flow meter | Hoffer | HO1/2X1/4A-.35-3.5-BP-1MX-MS-X |
| Pressure transducer | Omega | PX309-050A10V |
| Thermocouple module | National Instrument | NI-9213 |
| Target machine | Speedgoat | Performance real-time target machine |

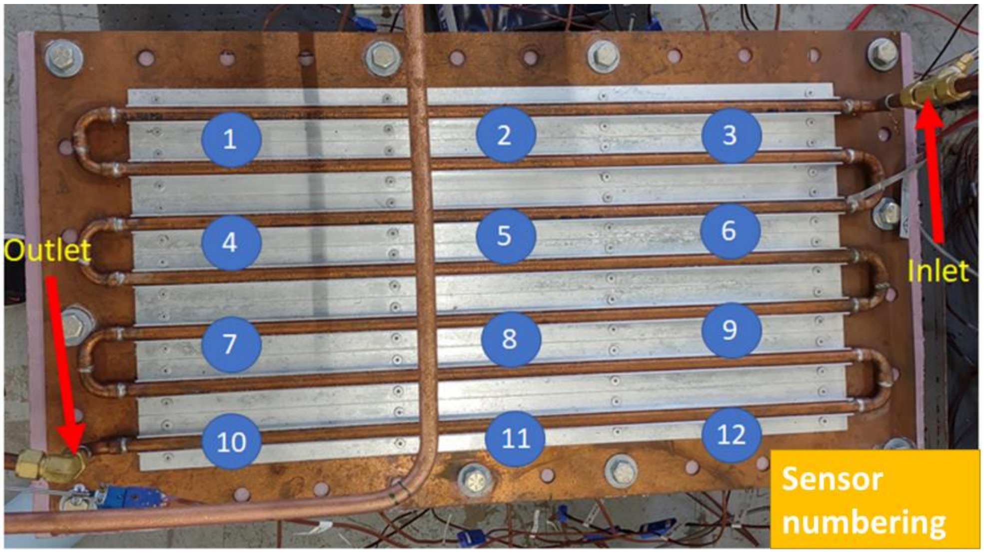


Figure 23. Thermocouple placement (under the panel) for panel surface temperature measurement.

The justification for selecting the aluminum panel over the copper one can be constructed on three factors which provide comprehensive outlook of the overall performance of the thermal transfer panel. The average surface temperature at the steady state provides an assessment of effectiveness in heat transfer between the solid and fluid. The range of temperature is an evaluation of the uniformity of the temperature distribution across the panel. Lastly, the time constant for convergence is the indicator of sensitivity and responsiveness of the panel to serve as the transfer system. To bring these behaviors forth from the thermal transfer panels, various setpoint combinations in “step” were used as the commands to the chiller. Figure 24 shows an example of such command and resulting behavior. As seen in the figure, the average surface temperature of the panels moves from one steady-state to another as a response of the step input change for the chiller. It can be noted that the dynamic response and steady-state temperatures of both copper and aluminum thermal panels are very similar.

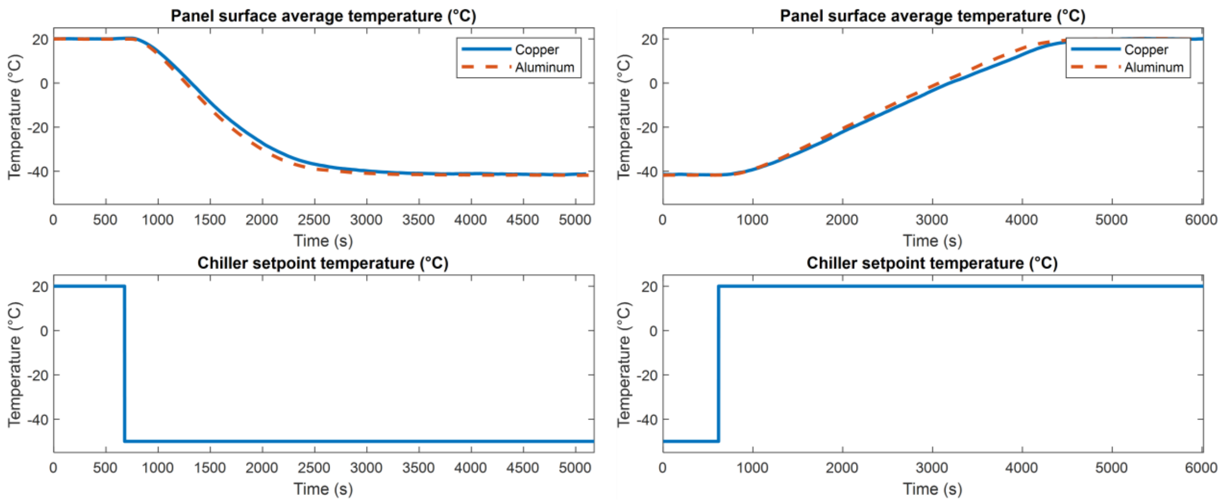


Figure 24. Dynamic behavior of average panel surface temperature for sudden drop and rise of setpoint temperature between 20 °C and -50 °C

To evaluate the uniformity of temperature profile, temperature recordings for the panel surface profile are organized into heatmaps as presented in Figure 25. It can be observed that for both versions of thermal transfer plates, temperature values are low within the central region compared to the outer region. This is due to diminishing effect of insulation toward the fringe of the panel and the absence of insulation along the perimeter of the panel. Combining the trials with other setpoints the results can be generalized as arranged in Table 9. Regarding the time constant and average panel temperature values, it can be concluded that there is no significant difference in performance. However, the temperature range varies noticeably depending on the material of panels.

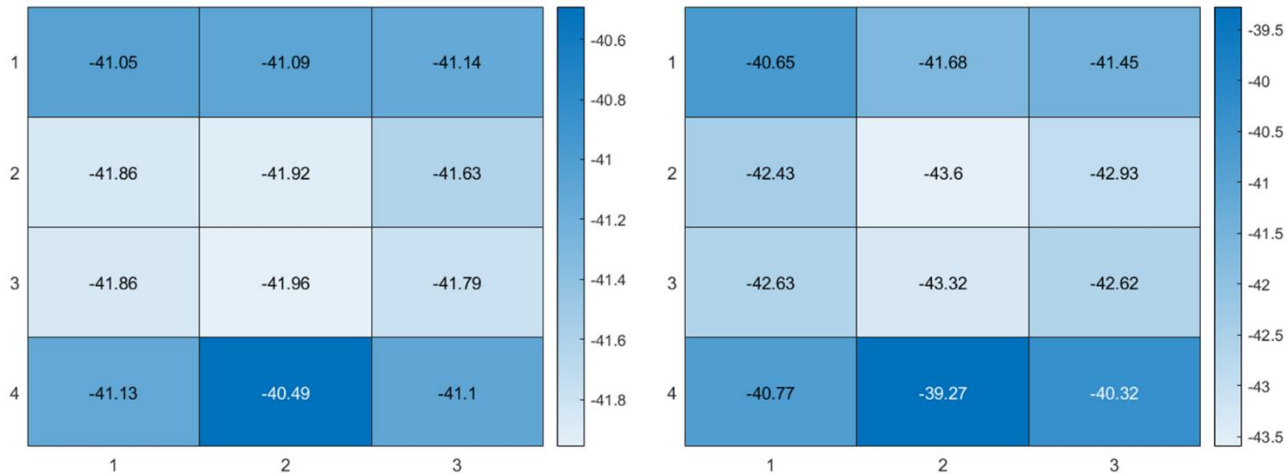


Figure 25. Steady-state temperature distribution of the panel surfaces at -50 °C fluid temperature (Left: Copper; Right: Aluminum; values are in Celsius)

Table 9. Summary of thermal transfer panel performance

| Trials (Setpoint) | Time Constant (s) | | Average Panel Temperature (°C) | | Temperature Range (°C) | |
|---|---|---|---|---|---|---|
| | Copper | Aluminum | Copper | Aluminum | Copper | Aluminum |
| 20 °C → -60 °C | 1267 | 1177 | -47.95 | -50.28 | 1.95 | 4.85 |
| 20 °C → -50 °C | 1063 | 988 | -41.42 | -41.81 | 1.47 | 4.33 |
| 20 °C → -30 °C | 808 | 753 | -24.08 | -24.38 | 1.14 | 3.37 |
| 20 °C → -10 °C | 606 | 559 | -6.57 | -7.26 | 0.78 | 1.71 |

*Notes: Time constant defined as the time it takes for the system to reach 0.63 of steady state value.*

With the results from the experimental data and requirements proposed by structural team of RETHi, it was concluded to be appropriate to compromise the uniformity in temperature profile over the weight of the thermal transfer panels. Therefore, the thermal transfer panels will have aluminum plate for full-size CPT setup. With the similar approach for optimization of geometry of the pipe layouts and meaningful data collected from the prototype experiments, a full-size thermal transfer panel, which has a triangular base, will be developed as the next step.

### 3.3 Small-scale Testbed: Pressure Box Testing

To expand the scope of prototype experiments outside of thermal transfer system, a new component, a pressurized metal box, is introduced. Pressurized with nitrogen gas at 14 psi above the atmosphere, the "pressure box" serves as a scaled-down representation of the structural system.

The interior of the box, nitrogen gas, is then considered to be the simplified portrayal of the interior environment. With the input command to the thermal transfer system from the computer, the experimental setup now captures all necessary components, physical, virtual, and transfer substructures for the CPT, although only in a simplified manner. Figure 26 presents the setup with the insulation layer removed between the thermal transfer panel and pressure box for physical, thermal coupling of the components. Additionally, a conceptual diagram is provided describing one way coupling of the CPT architecture in which virtual simulation results in cascading physical behavior through series of coupled systems.

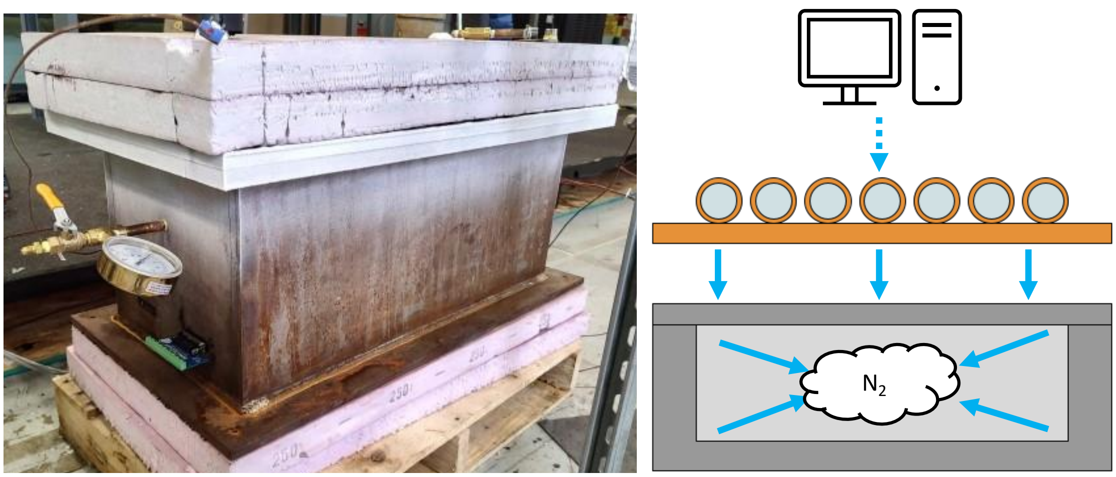


Figure 26. Addition of pressurized box and conceptual diagram of small-scale CPT

A similar experiment was conducted for the combined pressure box and thermal transfer panel test setup. Using the chiller input command to vary the temperature of the heat transfer fluid, the dynamic responses of the panel and interior air were recorded. Figure 27 shows how the temperatures of the thermal transfer panel and the air inside the box change over time when a step function command input is imposed. Compared to the previous experimental results when the thermal transfer panel was detached and isolated from the pressure box by the insulation pads, the shape of the curve for the average thermal panel temperature suggests that the system requires a significantly longer period to show a full convergence. When the setpoint change is triggered, the temperature of the panel starts to drop. However, after about 30 minutes, the rate of change for the temperature slows down dramatically. This trend continues while the temperature of interior air is reaching its convergence, whose dynamic is noticeably slower than the thermal transfer panel.

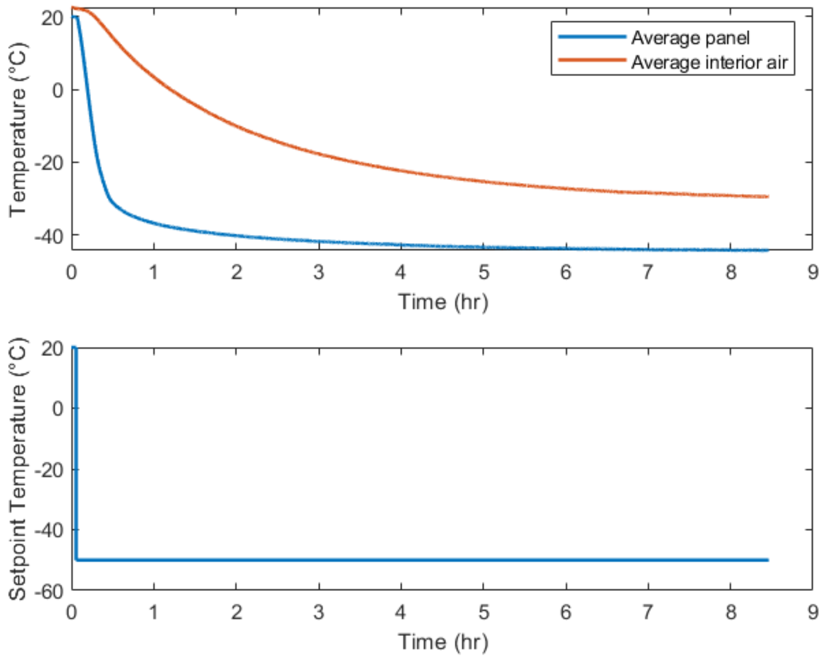


Figure 27. Dynamic behavior of thermal transfer panel and interior air temperature with step input command for chiller (-50 °C)

The confined air inside the pressurized box experiences gradual drop of pressure due to the change of temperature. Figure 28 shows the change of pressure throughout the testing. For further comparison, pressure drop estimation based on ideal gas assumption is provided. As the temperature change is the main driving factor of the pressure for the air, pressure takes a similar shape for its dynamic behavior. There seems to be a noticeable discrepancy between the measured pressure and the estimated pressure values. The two lines even display a sign of divergence toward the end of the test. The observation suggests that there may be a small leakage over time, which makes the estimation inaccurate, and slowing down the convergence of the pressure of the interior air. However, the unwanted leakage in the system alone does not seem to fully justify the disagreement between the measured and predicted values. A careful analysis is necessary to determine whether the assumption for ideal gas is acceptable.

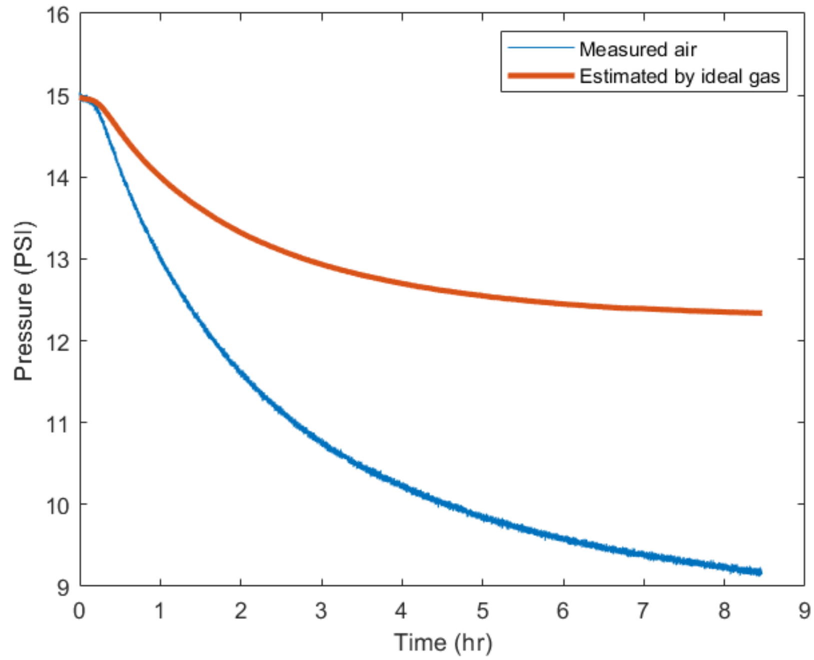


Figure 28. Dynamic behavior of interior air pressure compared to the theoretical pressure calculated from ideal gas law

The experiment was repeated for different command input for the chiller, -10 °C and -30 °C respectively. Figure 29 and Figure 30 summarizes the results for the two additional tests. Although the y-axis is in different scale for each of these cases, the general trend of the curve exhibits almost identical shape as a group. The temperature of the thermal transfer panel drops with a fast rate of change in the beginning of the test but decelerates drastically. For the pressure and temperature of the interior air, slow dynamics are still present similar to the previous results. The disagreement in theoretical prediction by the ideal gas assumption and the actual data persists, though in different magnitude.

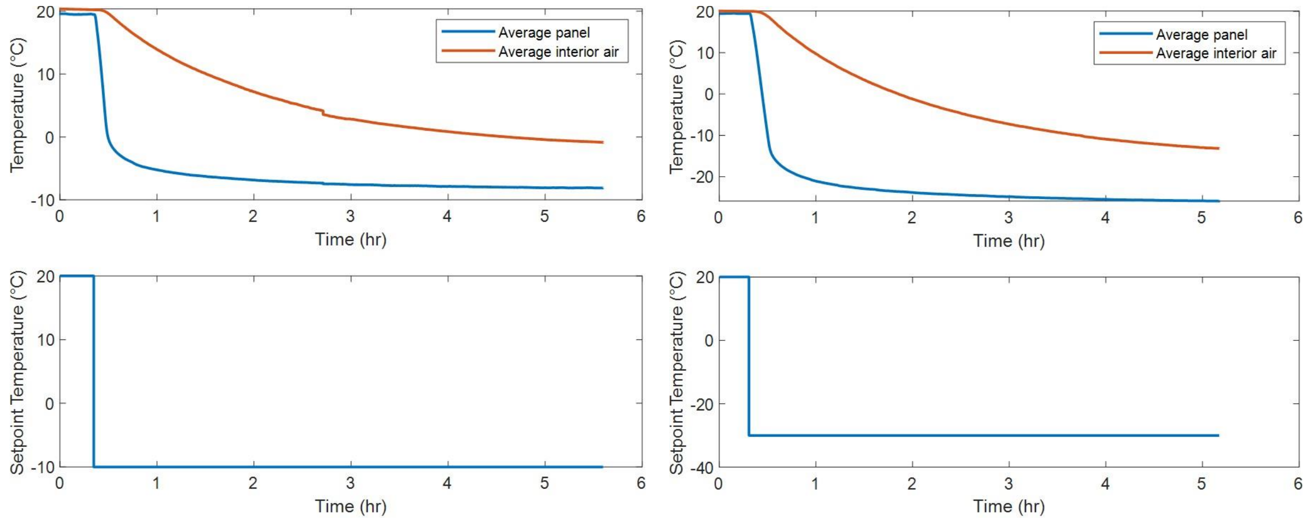


Figure 29. Dynamic behavior of thermal transfer panel and interior air with step input of -10 °C (left) and -30 °C (right)

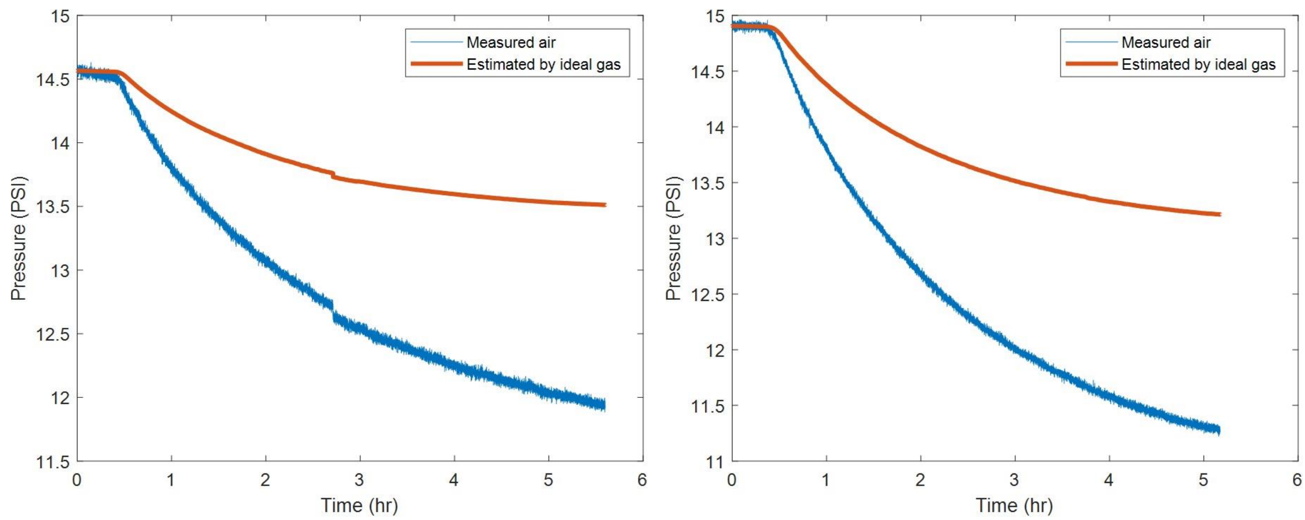


Figure 30. Dynamic behavior of interior air pressure compared to theoretical pressure with step input of -10 °C (left) and -30 °C (right). There is a loss of data for about 7 min for the plot on the left.

The ultimate functionality of thermal transfer system is to successfully transfer the information from the cyber substructure to the physical realization. Concerning the current architecture of the CPT, it is the panel surface temperature that represents the interface between cyber and physical substructures. Therefore, the next reasonable step is to conduct an analysis of control capability of the thermal transfer system. Figure 31 illustrates the feedback control loop involving PID controller. The control loop takes the desired temperature of the panel as an input and outputs the heat transfer fluid setpoint temperature to be received by the chiller, which also has its own internal control loop to operate the two-phase cycle for cooling of the heat transfer fluid. The desired panel temperature is determined by the result of numerical simulation in the cyber substructure according to the simulation scenarios concerning disturbances such as meteorite impact and solar radiation. For the following set of experiments, a sine wave of varying amplitude with 3-hr period was chosen as desired control setpoint for the purpose of demonstration.

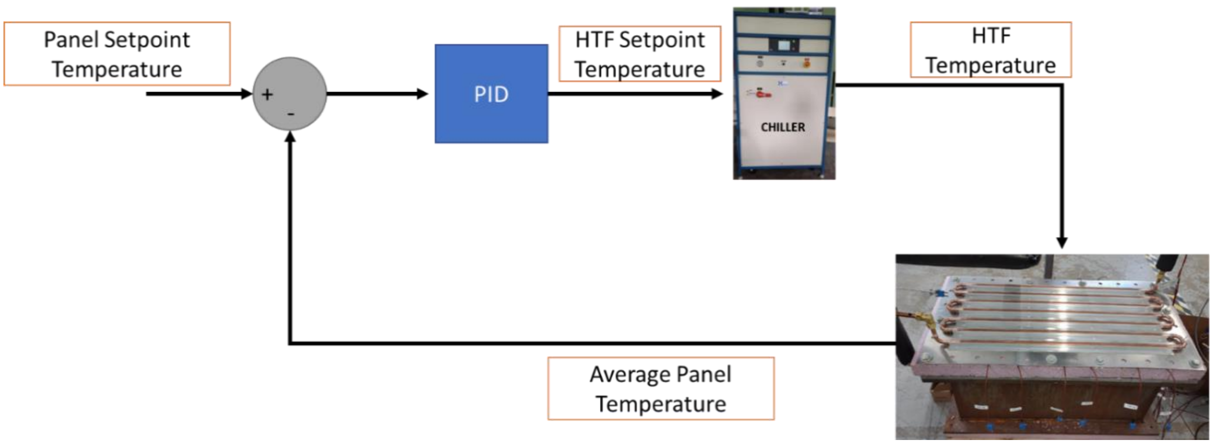


Figure 31. PID diagram for control feedback loop of thermal transfer system

Three different amplitude values for the sine wave, 50 °C, 30 °C, and 10 °C, were used. The results are presented in both Figure 32 and Figure 33. To aid with the performance evaluation of the controller, residuals in absolute scale are provided. For relatively narrower amplitudes, control cases with 10 °C and 30 °C result in maximum residuals of 1 °C and 2 °C respectively. However, for the case with 50 °C as an amplitude, the residuals become larger even up to 20 °C in some places. Although there is still a room for improvements by fine-tuning of the controller, it can be observed from the figure that the rate of change for the actual panel temperature is noticeably slower than that for the setpoint command. This implies that there exists a limit from the chiller whose performance, physically denoted as the outlet heat transfer fluid temperature, is saturated by finite bounds. Similarly, due to the internal control loop and other control schemes implemented by the manufacturer, the rate of change for the heat transfer fluid will be saturated as well. Another interesting observation is that the rate of change is slightly different depending on the direction (*i.e.*, cooling and heating). In other words, the negative rate of change is larger in magnitude than the positive rate of change. This is attributed to the fact that the cryogenic chiller uses different mechanisms to achieve cooling and heating of the heat transfer fluid. It uses two-phase refrigeration cycle in case of cooling but uses an electrical heater for heating. These types of physical or equipment-related limitations are to be identified and analyzed in more depth in forthcoming studies.

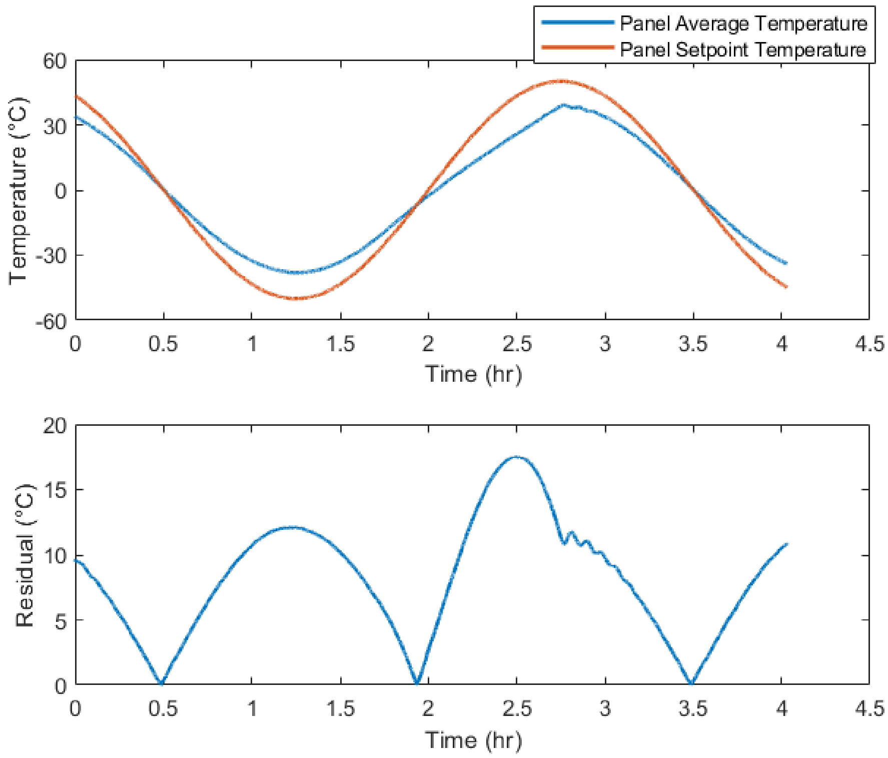


Figure 32. Control command input and physical output for thermal transfer panel for amplitude of 50 °C

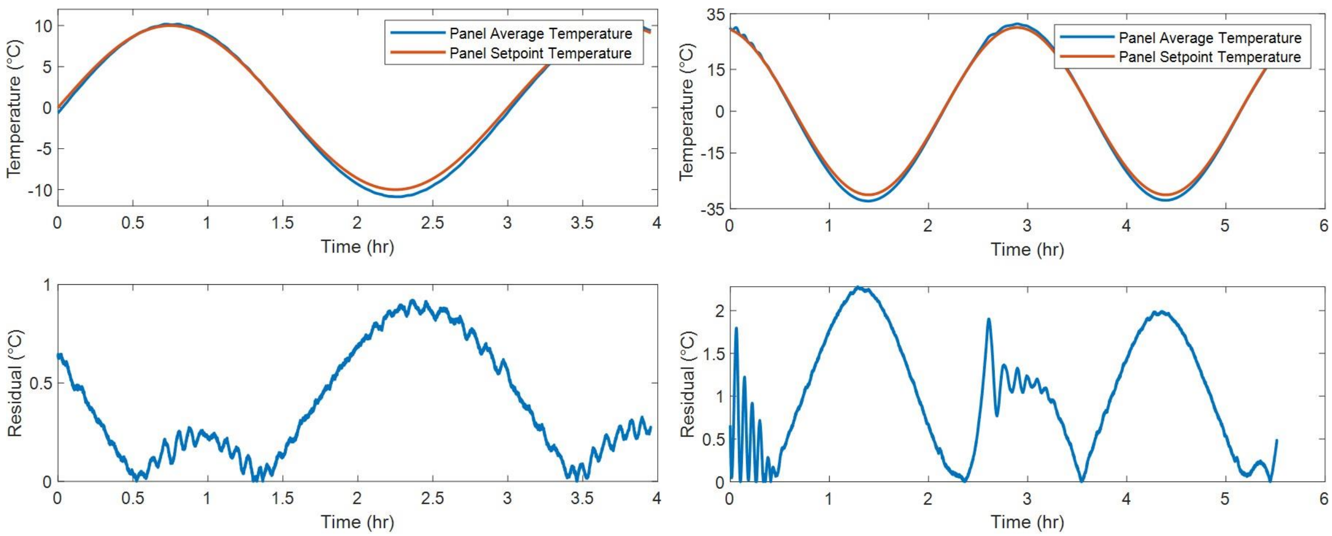


Figure 33. Control command input and physical output for thermal transfer panel for amplitude of 10 °C and 30 °C respectively

# 4. CONCLUSION, CHALLENGES AND FUTURE WORK

This work described the conceptualization and design of a Cyber-Physical Testbed (CPT) architecture to study future resilient habitats. As components of the physical substructure, the thermal and pressure management systems have been designed to be compatible and applicable to the other physical subsystems and the scope of testing scenarios. Detailed design considerations and performance mapping data were discussed for the thermal transfer system. To recreate the extra-terrestrial environmental conditions (*i.e.,* lunar regolith), a cryogenic chiller needed to be selected and commissioned. A comprehensive data acquisition platform was then required to bring various hardware and matching software into MATLAB/Simulink environment. To evaluate the reliability of the chiller commission and gain understanding of the system altogether, the performance of the chiller and thermal transfer panel was recorded at various input conditions.

As a result of the work, the chiller loop was successfully commissioned into the lab environment and confirmed to be functioning as expected. Data acquisition platform which embraces several different software and data transfer methods among hardware was developed and deployed. These hardware and software framework used for the presented work will be continuously employed for future work, the full-sized CPT. Performance mapping data were analyzed to provide valuable resources for system identification and control optimization. A small-scale CPT with a control loop implemented for the thermal transfer system was conducted. It was shown that the current design and approach for the thermal transfer system provided functionalities that were required for CPT, recreating the interface condition as a form of temperature boundary. Moreover, cascading effect induced by the thermal transfer system through the physical substructure was observed. However, for certain simulation conditions and scenarios, the current setup has shown to have a limited capacity. The future work would spread out into two main branches of tasks: expansion of the pressure box testing and full-size dome commissioning.

Continuous effort is required to address some of the unanswered questions. One important question would be how to measure or calculate the heat flux to close the loop between the cyber and physical substructure. One potential point of investigation is to measure the inlet and outlet heat transfer fluid across the panel. This way, it would be possible to calculate how much heat was gained or lost through the serpentine-like loops of the heat transfer fluid, providing an estimate of the heat flux for the thermal transfer panels. Another method would be solving inverse heat transfer problem by obtaining temperature values through the depth of the thermal transfer panel. For this approach, placement of thermocouple would be a challenge since it has a risk of undermining surface contact quality between the thermal transfer panels and the surface of the structural system. With respect to the pressure box, minimizing unintended leakage, whether it is pressure related or thermal related, is critical to the success of the testing. Once there is an affirmation that there are no significant unwanted disturbances, it would be interesting to further complicate the testing scenarios by introducing intended disturbances. One example would be a controlled leakage in the system. As the leakage is intentionally induced, it would be monitored and brought into the analysis following the experiments. A bit different in its nature, a heat source can be installed within the pressure box as an internal disturbance. Within the context of the CPT, this would be a representation of fire or excessive heat generation from equipment. Further efforts made surrounding the pressure box setup would provide meaningful lesson which can be then taken to the full-size CPT setup development.

Working in harmony with various teams concerning the development of the physical substructure of CPT, design iterations for thermal transfer panel should continue. The imminent work effort is to be focused on developing a triangular thermal transfer panels to be compatible with the current design of the structural system. Since the full-size CPT would host multiple thermal transfer panels of such design, a careful plan is to be laid out for constructing pipe network which would eventually form a loop with the inlet and outlet ports of the chiller. It is then also a matter of great importance to develop a controller or a group of controllers to ensure the localization of damage by controlling each panels individually. One potential way to achieve this is to place a bypass loop per panel so that the amount of heat transfer fluid can be controlled individually. Another method to consider is having a secondary loop for the heat transfer fluid which would be maintained at high temperature. By mixing the hot and cold heat transfer fluid, the desired fluid temperature for panels can be achieved without much delay.

# APPENDIX

## Equipment used for physical systems

Table (Appendix) 1. List of sensors and hardware used for thermal management system

| Equipment | Manufacturer | Model |
|---|---|---|
| Thermocouple | Industrial Process and Sensor | T-20-TT |
| Thermocouple probe | Industrial Process and Sensor | TG20T0142U00600MP |
| Flowmeter | Omega | FTB-1423-AMP |
| Anemometer | Omega | FMA904R-V1 |
| Heat pump | Water Furnace | LDH024*104CSL2AN |
| Water Pump | Taco Pump | SKV1507D-1760-1.5 |
| Radiator Coil | Outdoor Furnace Supply | HWC-8X8 |
| Radiator Fan | Auto Dynasty | AD-RAF-9-BL+FMK |

Table (Appendix) 2. List of sensors and hardware used for pressure management system

| Equipment | Manufacturer | Model |
|---|---|---|
| Thermocouple | Industrial Process and Sensor | T-20-TT |
| Thermocouple probe | Industrial Process and Sensor | TG20T0142U00600MP |
| Control valve | Kelly Pneumatics | KPIM-VP-10-A0-156-V |
| Air flow meter | Kelly Pneumatics | KPI-AMFS-1-A |
| Pressure controller | Omega | EP211-X120-10V |
| Pressure regulator & dryer | McMaster-Carr | 3274N11 |

# REFERENCES


[1] M. Vijayan, A. Patil, and V. Kapse, "Assessing the Evolution of Human Settlements with 'Energy' as a Determinant," *EDP Sciences*, vol. 140, no. E3S Web of Conferences, p. 01010, 2020, doi: 10.1051/conf/202017001010.

[2] A. D. Moore, P. A. Lynn, A. H. Feiveson, and J. M. Reeves, "The first 10 years of aerobic exercise responses to long-duration ISS flights," *Aerospace Medicine and Human Performance*, vol. 86, pp. A78–A86, Dec. 2015, doi: 10.3357/AMHP.EC10.2015.

[3] M. Chen, R. Goyal, M. Majji, and R. E. Skelton, "Review of space habitat designs for long term space explorations," *Progress in Aerospace Sciences*, vol. 122, Apr. 2021, doi: 10.1016/j.paerosci.2020.100692.

[4] S. Bishop and S. Hahäuplik-Meusburger, *Space and Society Series Editor-in-Chief: Space Habitats and Habitability Designing for Isolated and Confined Environments on Earth and in Space*. Springer International Publishing, 2021. [Online]. Available: http://www.springer.com/series/11929

[5] O. Almirall Toribio *et al.*, *The Moon: The Next International Space Station*. Iniciativa Digital Politècnica. Oficina de Publicacions Acadèmiques Digitals de la UPC, 2020.

[6] "Lunar Surface Innovation Consortium," *The Johns Hopkins University Applied Physics Laboratory LLC.*, 2022. https://lsic.jhuapl.edu/ (accessed Apr. 18, 2022).

[7] "HOME: Habitats Optimized for Missions of Exploration," *Space Technology Research Institute*, Sep. 09, 2021. https://homestri.ucdavis.edu/ (accessed Apr. 18, 2022).

[8] "RETH: Resilient ExtraTerrestrial Habitats," *Purdue University*, 2022. https://www.purdue.edu/reth/ (accessed Apr. 18, 2022).

[9] S. J. Dyke, K. Marais, I. Bilionis, J. Werfel, and R. Malla, "Strategies for the design and operation of resilient extraterrestrial habitats," 2021. doi: 10.1117/12.2585118.

[10] X. Li, A. I. Ozdagli, S. J. Dyke, X. Lu, and R. Christenson, "Development and Verification of Distributed Real-Time Hybrid Simulation Methods," *Journal of Computing in Civil Engineering*, vol. 31, no. 4, p. 04017014, Jul. 2017, doi: 10.1061/(asce)cp.1943-5487.0000654.

[11] X. Wang, R. E. Kim, O.-S. Kwon, I.-H. Yeo, and J.-K. Ahn, “Continuous Real-Time Hybrid Simulation Method for Structures Subject to Fire,” *Journal of Structural Engineering*, vol. 145, no. 12, p. 04019152, Dec. 2019, doi: 10.1061/(asce)st.1943-541x.0002436.

[12] C. A. Whyte, K. R. Mackie, M. Asce, and B. Stojadinovic, “Hybrid Simulation of Thermomechanical Structural Response,” *Journal of Structural Engineering*, vol. 142, no. 2, 2015, doi: 10.1061/(ASCE)ST.1943.

[13] C. Park, P. A. Reneke, M. A. Galler, S. T. Bushby, and W. D. Davis, “Enhancement of the virtual cybernetic building testbed to include a zone fire model with HVAC components,” Gaithersburg, MD, 2007. doi: 10.6028/NIST.IR.7414.

[14] A. Maghareh, J. P. Waldbjørn, S. J. Dyke, A. Prakash, and A. I. Ozdagli, “Adaptive multi-rate interface: development and experimental verification for real-time hybrid simulation,” *Earthquake Engineering and Structural Dynamics*, vol. 45, no. 9, pp. 1411–1425, Jul. 2016, doi: 10.1002/eqe.2713.

[15] A. Maghareh, S. Dyke, S. Rabieniaharatbar, and A. Prakash, “Predictive stability indicator: a novel approach to configuring a real-time hybrid simulation,” *Earthquake Engineering and Structural Dynamics*, vol. 46, no. 1, pp. 95–116, Jan. 2017, doi: 10.1002/eqe.2775.

[16] A. Maghareh *et al.*, “A Reflective Framework for Performance Management (REFORM) of Real-Time Hybrid Simulation,” *Frontiers in Built Environment*, vol. 6, Sep. 2020, doi: 10.3389/fbuil.2020.568742.

[17] A. Maghareh, C. E. Silva, and S. J. Dyke, “Parametric model of servo-hydraulic actuator coupled with a nonlinear system: Experimental validation,” *Mechanical Systems and Signal Processing*, vol. 104, pp. 663–672, May 2018, doi: 10.1016/j.ymssp.2017.11.009.

[18] A. V. S. Oliveira, A. Avrit, and M. Gradeck, “Thermocouple response time estimation and temperature signal correction for an accurate heat flux calculation in inverse heat conduction problems,” *International Journal of Heat and Mass Transfer*, vol. 185, Apr. 2022, doi: 10.1016/j.ijheatmasstransfer.2021.122398.

[19] F. Lin, A. Maghareh, S. J. Dyke, and X. Lu, “Experimental implementation of predictive indicators for configuring a real-time hybrid simulation,” *Engineering Structures*, vol. 101, pp. 427–438, Oct. 2015, doi: 10.1016/j.engstruct.2015.07.040.

[20] A. Maghareh, C. E. Silva, and S. J. Dyke, "Servo-hydraulic actuator in controllable canonical form: Identification and experimental validation," *Mechanical Systems and Signal Processing*, vol. 100, pp. 398–414, Feb. 2018, doi: 10.1016/j.ymssp.2017.07.022.

[21] A. Sauca, E. Mergny, T. Gernay, and J. M. Franssen, "A method for hybrid fire testing: Development, implementation and numerical application," *Applications of Fire Engineering*, 2018.

[22] S. Renard, J. C. Mindeguia, F. Robert, S. Morel, and J. M. Franssen, "An Adaptive Controller for Hybrid Fire Testing," *Experimental Techniques*, vol. 44, no. 6, pp. 701–714, Dec. 2020, doi: 10.1007/s40799-020-00369-6.

[23] N. D. Pope and C. G. Bailey, "Quantitative comparison of FDS and parametric fire curves with post-flashover compartment fire test data," *Fire Safety Journal*, vol. 41, no. 2, pp. 99–110, Mar. 2006, doi: 10.1016/j.firesaf.2005.11.002.

[24] A. Maghareh, A. Lenjani, M. Krishnan, S. Dyke, and I. Bilionis, "Role of Cyber-Physical Testing in Developing Resilient Extraterrestrial Habitats," 2021. doi: 10.1061/9780784483374.098.

[25] C. Pan, D. Ziviani, and J. E. Braun, "Performance evaluation of a vapor-compression-cycle based heat pump system for a lunar habitat under the impact of dust deposits on the coupled radiators," *Acta Astronaut*, vol. 194, pp. 22–33, 2022, doi: 10.1016/j.actaastro.2022.01.040.

[26] F. P. Incropera, *Fundamentals of heat and mass transfer.*, 6th ed. / Frank P... Hoboken, NJ: John Wiley, 2007.

[27] I. H. Bell, J. Wronski, S. Quoilin, and V. Lemort, "Pure and Pseudo-pure Fluid Thermophysical Property Evaluation and the Open-Source Thermophysical Property Library CoolProp," *Ind Eng Chem Res*, vol. 53, no. 6, pp. 2498–2508, 2014, doi: 10.1021/ie4033999.

[28] S. W. Churchill and H. H. S. Chu, "Correlating equations for laminar and turbulent free convection from a vertical plate," *International Journal of Heat and Mass Transfer*, vol. 18, no. 11, 1975, doi: 10.1016/0017-9310(75)90243-4.

[29] B. Bueno, L. Norford, G. Pigeon, and R. Britter, "A resistance-capacitance network model for the analysis of the interactions between the energy performance of buildings and the urban climate," *Build Environ*, vol. 54, pp. 116–125, 2012, doi: 10.1016/j.buildenv.2012.01.023.

[30] M. de Rosa, V. Bianco, F. Scarpa, and L. A. Tagliafico, "Impact of wall discretization on the modeling of heating/cooling energy consumption of residential buildings," *Energy Effic*, vol. 9, no. 1, pp. 95–108, 2015, doi: 10.1007/s12053-015-9351-5.

[31] M. Sameti and A. Kasaeian, "Numerical simulation of combined solar passive heating and radiative cooling for a building," *Build Simul*, vol. 8, no. 3, pp. 239–253, 2015, doi: 10.1007/s12273-015-0215-x.

[32] B. Torregrosa-Jaime, F. Bjurling, J. M. Corberán, F. di Sciullo, and J. Payá, "Transient thermal model of a vehicle's cabin validated under variable ambient conditions," *Appl Therm Eng*, vol. 75, pp. 45–53, 2015, doi: 10.1016/j.applthermaleng.2014.05.074.

[33] J. Wu, F. Jiang, H. Song, C. Liu, and B. Lu, "Analysis and validation of transient thermal model for automobile cabin," *Appl Therm Eng*, vol. 122, pp. 91–102, 2017, doi: 10.1016/j.applthermaleng.2017.03.084.

[34] R. W. Fox, *Fox and McDonald's introduction to fluid mechanics.*, 8th ed. / Philip ... Hoboken, NJ: John Wiley & Sons, Inc., 2011.

[35] M. Carello, A. Ivanov, and L. Mazza, "Pressure Drop In Pipe Lines For Compressed Air:comparison Between Experimental And Theoretical Analysis," *WIT Transactions on Engineering Sciences*, vol. 18, 1998, doi: 10.2495/AFM980041.

[36] L. SIMONSEN, M. DEBARRO, and J. FARMER, "Conceptual design of a lunar base thermal control system," 1992.

[37] X. Mo, H. Zhi, Y. Xiao, H. Hua, and L. He, "Topology optimization of cooling plates for battery thermal management," *International Journal of Heat and Mass Transfer*, vol. 178, Oct. 2021, doi: 10.1016/j.ijheatmasstransfer.2021.121612.

[38] M. Kilic, M. Aktas, and G. Sevilgen, "Thermal assessment of laminar flow liquid cooling blocks for LED circuit boards used in automotive headlight assemblies," *Energies (Basel)*, vol. 13, no. 5, Mar. 2020, doi: 10.3390/en13051202.

[39] M. R. Saffarian, M. Moravej, and M. H. Doranehgard, "Heat transfer enhancement in a flat plate solar collector with different flow path shapes using nanofluid," *Renewable Energy*, vol. 146, pp. 2316–2329, Feb. 2020, doi: 10.1016/j.renene.2019.08.081.

[40] Michael K. Ewert, Patricia A. Petete, and John Dzenitis, "Active Thermal Control Systems for Lunar and Martian Exploration," *SAE transactions*, vol. 99, pp. 613–623, 1990.

[41] "SolidWorks Flow Simulation." Dassault Systèmes, Vélizy-Villacoublay, France, 2020.

# VITA

Jaewon Park was born in 1995 in Seoul, South Korea. He graduated from Bucknell University, Lewisburg, Pennsylvania, with bachelor's degree in mechanical engineering in 2020. During his undergraduate education, he was involved in research in the dynamics of human body motion. As a bodybuilding and calisthenics enthusiast, he explored novel methods to achieve classification of correct and wrong forms during bench press exercises with data driven algorithms using limited number of inertial measurement units (IMUs) attached on human patients' bodies. He started the Master's in Science and Mechanical Engineering (MSME) program at the Purdue University in West Lafayette, Indiana in fall 2020. As a student member of the Resilient Extra-terrestrial Habitat Institute (RETHi), he focused on developing a framework of real-time hybrid simulation testing for deep space habitats. At Ray W. Herrick Laboratories in West Lafayette, Indiana, he laid a groundwork for the commissioning the physical substructure and transfer system for the Cyber-Physical Testbed of RETHi. He plans to continue his academic pursuit at Purdue as a PhD candidate.

# PUBLICATIONS

**TFAWS 2021 Thermal and Fluid Analysis Workshop**

Development of a Virtual Cyber-Physical Testbed for Resilient Extra-Terrestrial Habitats

Jaewon Park*, Herta Montoya, Yuguang Fu, Amin Maghareh, Shirley J. Dyke, Davide Ziviani, Conference Presentation, Virtual

**2021 IAC Poster**

Development of a Virtual Cyber-Physical Testbed for Resilient Extra-Terrestrial Habitats

Jaewon Park, Herta Montoya, Laura Collazo Carbullude, Amanda Lial, Poster Presentation, Purdue University

**SEAC Conference**

Inside Resilient Extraterrestrial Habitats

Shirley Dyke, Herta Montoya, Jaewon Park, Zixin Wang, Conference Presentation, Indianapolis, IN